Iron based Li-ion insertion materials for battery applications

Abstract

Li-ion batteries are currently the most efficient technology available for electrochemical energy storage. The technology has revolutionized the portable electronics market and is becoming a corner stone for large scale applications, such as electric vehicles. It is therefore important to develop materials in which the energy storage relies on abundant redox active species, such as iron. In this thesis, new iron based electrode materials for positive electrodes in Li-ion batteries were investigated. Lithium iron pyrophosphate ($Li_2FeP_2O_7$) and two polymorphs of lithium iron sulphate fluoride ($LiFeSO_4F$) were studied.

For $Li_2FeP_2O_7$, preferred oxidation of iron with different coordination numbers within the crystal structure was studied, and six-coordinated iron was found to be oxidized preferentially at lower potentials compared to five-coordinated iron. Electrochemical cycling resulted in structural changes of $Li_2FeP_2O_7$ through an increased Li-Fe mixing in the compound, forming a metastable state during battery operation.

For *tavorite* $LiFeSO_4F$, the influence of the amount of a conductive polymer (poly(3,4-ethylenedioxythiophene), or PEDOT) was studied. All the different amounts of PEDOT coating reduced the polarization significantly, but the trade-off between functionality and weight added also has to be considered. Additionally, the effect of densifying the electrodes to different degrees is reported, and was found to have a significant influence on the battery performance. Also *triplite* $LiFeSO_4F$ was coated with PEODT, and it was found that the electrochemical performance improved, but not to the same extent as for *tavorite* $LiFeSO_4F$. The faster solid state transport of Li-ions in *tavorite* type $LiFeSO_4F$ possibly accounts for the difference in electrochemical performance.

Together, the results presented herein should be of importance for developing new iron based materials for Li-ion batteries.

Sammanfattning på svenska

Av de idag tillgängliga teknologierna för elektrokemisk energilagring så har litium-jonbatterier de bästa egenskaperna när det gäller energiförluster och energilagringskapacitet. De har revolutionerat marknaden för portabel elektronik (telefoner, laptops etc.), och blir mer och mer viktiga för storskaliga tillämpningar såsom elbilar. För den typen av applikationer måste teknologin baseras på vanligt förekommande material och grundämnen, t.ex. järn.

I den här avhandlingen har järnbaserade material för den positiva elektroden hos litium-jonbatterier studerats. Olika aspekter som påverkar spänningen och effektiviteten hos elektroderna har undersökts. Ett exempel på det är hur olika omgivningar kring järnatomerna i en förening påverkar spänningen hos ett batteri. För föreningen litiumjärnpyrofosfat visade det sig att sex närmaste grannar ger lägre spänning än fem närmaste grannar till järn. Dessutom har förändringar i föreningens struktur studerats då den används i ett batteri. Den här typen av grundforskning är viktig för förståelsen av nya elektrodmaterial i Li-jonbatterier.

Ur en mer praktisk synvinkel så har elektroder baserade på en annan järnförening, litiumjärnsulfatfluorid, utvecklats. Ledningsförmågan hos dessa elektroder har förbättrats genom att belägga föreningen med ett ledande skikt, samt att mekaniskt pressa samman elektroderna genom mangling. Båda metoderna är viktiga för att tillverka välfungerande elektroder. Föreningen litiumjärnsulfatfluorid förekommer i två olika former, och en jämförelse av hur elektriskt ledande beläggningar påverkar de bägge materialen har också gjorts i den här avhandlingen.

Tillsammans visar resultaten från de olika studierna på hur man kan arbeta och tänka kring utvecklingen av nya material för litium-jonbatterier.

List of papers

This thesis is based on the following Papers, which are referred to in the text by their Roman numerals.

I Blidberg, A., Häggström, L., Ericsson, T., Tengstedt, C., Gustafsson, T., Björefors, F. (2015) **Structural and Electronic Changes in $Li_2FeP_2O_7$ during Electrochemical Cycling.** *Chemistry of Materials*, 27: 3801–3804

II Blidberg, A., Sobkowiak, A., Tengstedt, C., Valvo, M., Gustafsson, T., Björefors, F. (2016) **Battery performance of PEDOT coated $LiFeSO_4F$ Cathodes with controlled porosity.** *Submitted*.

III Sobkowiak, A., Blidberg, A., Tengstedt, C., Edström, K., Gustafsson, T., Björefors, F. **Investigating the Electrochemical Performance of PEDOT-coated *Triplite*-Type $LiFeSO_4F$ Cathode Material.** *In Manuscript*.

Reprints were made with permission from the respective publishers.

My contribution to the papers

I. Planned all the work, synthesized the materials, and conducted the electrochemical and crystallographic investigations. Took part in the Mössbauer experiments and data analysis. Wrote the manuscript with input from the co-authors.

II. Carried out the electrochemical characterizations, TGA, and XRD analysis. Planned the experiments and synthesized the materials, partly together with the second author. Took part in the XPS, SEM, FT-IR, and Raman characterization. Wrote the manuscript with input from the co-authors.

III. Carried out some of the electrochemical evaluation, gave input in developing the material synthesis conditions and designing the experiments. Drew some of the figures, wrote the experimental section, and gave input to the remaining parts of the manuscript.

Contents

Every answer gives rise to
ten new questions

1 Background

The World's energy use is dominated by the use of fossil fuel; in 2011 renewable energy sources accounted for less than 14% of the total energy supply.[1] From an environmental, political, and economic point of view there has been an interest in reducing the dependence on energy from fossil and finite resources and increasing the renewable part. The dominance of fossil fuels in the energy sector is visualized in *Figure 1*.

The transport sector is one of the largest energy users. In Sweden, the transport sector accounted for 23% of the total energy use during 2012. Only 11% of the energy used for transportation was converted from biofuels, waste or electricity. Corresponding numbers for the whole world are 28% of the total energy consumption in the transport sector with less than 4% biofuel, waste and electricity.[2] However, with an increasing use of intermittent energy sources, such as solar and wind power, larger demands are put on controlling the electric grid. Buffer capacity, *e.g.* battery systems, is required to even out fluctuations in electricity generation.[3–5] Synergetic effects with a plausible electrification of the transport sector also open up possibilities for such energy buffers, with increasing numbers of electric and plug-in electric vehicles integrating with smart electric grids.[6] The key component in such scenarios is likely the battery.

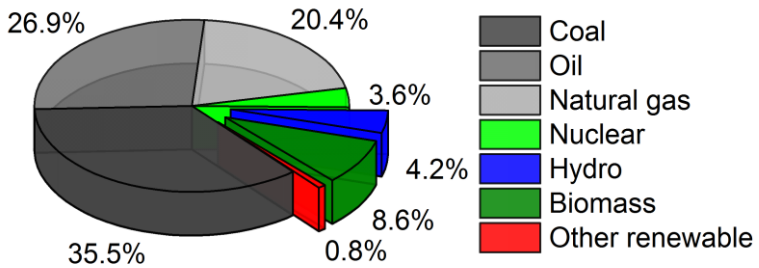

Figure 1. Distribution of the world's energy use as of the year 2011.[1] Renewable energy sources are shown with exploded wedges.

2 The Li-ion battery

Li-ion batteries by far outperform any other battery technology currently available in terms of energy storage capacity and cyclability.[7,8] For example, Li-ion batteries can store twice the amount of energy per weight unit compared to nickel-metal hydride batteries, and five times the amount compared to lead-acid batteries.[7] The working principle of a Li-ion battery relies on insertion materials. In such materials a guest ion, such as Li^+, can be inserted and extracted reversibly into a crystalline host framework for thousands of cycles. At the positive electrode, referred to as *cathode* in the battery literature, Li^+ is used to balance the charge of redox active species, such as the $Fe^{3+/2+}$ redox couple. When iron is reduced from +III to +II by an electron from the outer circuit, Li^+ is inserted into the material to maintain the charge balance. *Vice versa*, when iron is oxidized back to +III, Li^+ is extracted from the material. For the negative electrode, labelled *anode* in the battery literature, carbon based materials are commonly used.[9] Upon electrochemical cycling, Li-ions are intercalated and extracted between the graphene sheets in the graphite structure. In this way, Li^+ travels back and forth between insertion materials at the positive and the negative terminals. Thus, the technology is sometimes referred to as the "Rocking Chair Battery".[7,10] Often in battery research, only one of the electrodes is studied at a time. Then lithium metal in large excess is used as a counter electrode. The working principle of an insertion electrode in such a *half-cell* is shown in *Figure 2*.

2.1 The development of commercial insertion cathodes

The insertion of a guest species into a crystalline host framework, the basis of the Rocking Chair Battery, was discovered in the 1970's.[11] The idea was to introduce a redox active species, such as a transition metal ion, into an ionically and electronically conductive material.[12] Fast sodium-ion conduction in the solid state had recently been reported for β-alumina, $Na_2O{\cdot}11Al_2O_3$,[13] and at that time the focus was on sodium-sulfur batteries.[3] The battery configuration consisted of liquid sodium as negative electrode, liquid sulfur at the positive terminal, and solid β-alumina as the electrolyte. Difficulties in handling liquid sodium motivated the use of solid electrodes

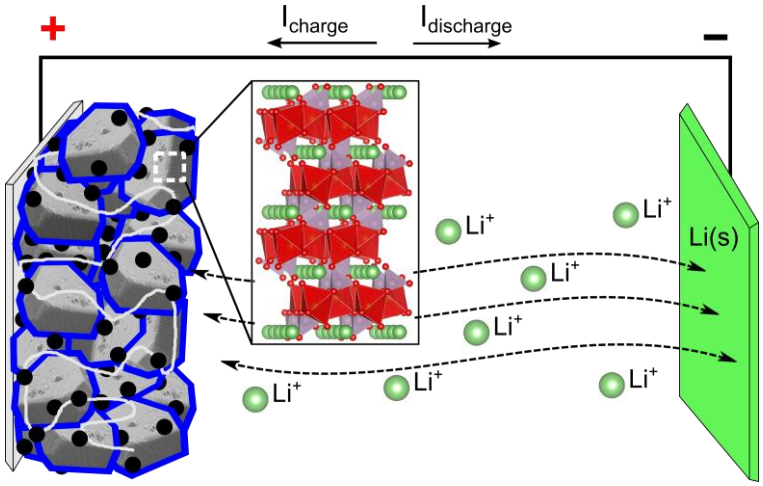

Figure 2. A typical half-cell configuration with a Li-ion insertion working electrode and a lithium metal counter electrode. The working electrode contains a Li-ion insertion material (structure shown as inset), with a conductive coating (blue), binder (light gray), and conductive additive (black) cast onto an Al current collector.

for measuring the ionic conductivity of β-alumina.[12] Sodium tungsten bronzes (Na_xWO_3) operating based on the $W^{6+/5+}$ redox couple, showed both high electronic conductivity and fast sodium-ion transport, and were used as electrode material for electrochemical characterization of β-alumina.[14] Thus, research on insertion electrode materials was initialized.

Focus soon shifted towards Li-ion batteries, due to the small ionic radius and light weight associated with Li-ions. The small ionic radius makes the Li-ion suitable for insertion into a crystalline framework, and the light weight is advantageous for the gravimetric energy density. The cell voltage is also high when Li is used as the negative electrode, due to the low standard potential of the Li^+/Li redox couple. TiS_2 and other metal chalcogenides (consisting of transition metals and later elements in group 16 of the periodic table) were investigated in the early cathode material research.[15,16] TiS_2 showed stable electrochemical cycling performance and high energy efficiency, attributed to the minor changes in the crystalline host during electrochemical cycling. No strong chemical bonds are broken in the crystalline framework during the insertion process, which is typical for Li-ion electrodes. Thus, only a slight mechanical stress is experienced by the electrode during operation, attributed to a slight expansion and contraction of the material during Li-ion insertion and extraction. The volume change can be explained by shorter *M*-*X* bonds in the material when metal ion M^{n+} has a higher charge, which pulls the negatively charged *X*-ligands closer.

TiS_2 batteries with lithium metal as the negative electrode were also commercialized,[12,15,17] but dendrite formation on the lithium anode caused battery failure and made them unsafe.[18] Additionally, TiS_2 is air sensitive

and must be handled in oxygen-free environments, complicating large scale battery manufacturing processes. Replacing the lithium metal with lithium alloys, such as LiAl,[19] were attempted to circumvent dendrite formation, but were disregarded due to capacity fading believed to be caused by the large volume expansion during the alloying reaction.[20]

The problems related to dendrite formation were overcome by combining an insertion cathode material in its discharged state, *i.e.* already lithiated after synthesis, with graphite as an insertion anode. This battery concept was realized by the discovery of $LiCoO_2$ in 1980,[21] and reversible intercalation into graphite in 1983.[22] Regarding the cathode material, the smaller oxide anion with its higher electronegativity also gave the advantage of higher operating voltage and capacity of $LiCoO_2$ compared to TiS_2. Essential for the reversibility of the graphite electrode is the use of ethylene carbonate (EC) as a solvent component. EC decomposes during the first charge process to form a passive film on graphite, which provides protection against further electrolyte decomposition and degradation.[23] A stable solid-electrolyte interface (SEI) is then formed.[24] The first Li-ion battery was commercialized by Sony in 1991,[25] and research on Li-ion batteries intensified.

Although $LiCoO_2$ ("LCO") was successfully used for commercial Li-ion batteries in the early 1990's, the scarcity of Co makes it desirable to replace it with more abundant elements,[26] *e.g.* Ni, and notably Mn and Fe.[27] Following the success of LCO, other members of the A_xMO_2 family were investigated. They all have a close-packed oxygen structure, with *M* metal ions in octahedral sites forming $(MO_2)_n$ layers. Alkali ions *A* are located between these sheets, and their coordination number depends on how the $(MO_2)_n$ layers are packed in the specific compounds.[28] Layered $LiNiO_2$, or more accurately $Li_{1-z}Ni_{1+z}O_2$, is iso-structural to $LiCoO_2$ but with a substantial occupancy of Ni in the Li-ion layers. These Ni-ions impede Li-ion insertion upon cycling, resulting in suboptimal electrochemical performance.[29] Co doping has been identified as a way of avoiding Ni-ion occupancy in the lithium layers.[30] Another disadvantage of Li_xNiO_2 is its poor thermal stability when delithiated and the risk of oxygen evolution also makes it unsafe. It was shown that Al doping can alleviated these problems,[31] and a combination of both cobalt and aluminum doping resulted in stable electrochemical performance as well as high thermal stability.[32] The "NCA" material, typically $LiNi_{0.8}Co_{0.15}Al_{0.05}O_2$,[33] is one of the cathode materials used in commercial Li-ion batteries today. Solid solutions of Li_2MnO_3 with $LiNiO_2$, just like aluminum doping, improved the thermal stability and safety of delithiated $LiNiO_2$.[34] "NMC" cathodes, or $LiNi_{1/3}Mn_{1/3}Co_{1/3}O_2$,[35,36] are together with NCA cathodes the current state-of-the art active materials for Li-ion batteries. They both operate on average at 3.7 V relative Li^+/Li and their practical capacities are 185 and 170 mAh/g, respectively. NMC has the best thermal stability, but NCA provides the fastest electron and Li-ion transport for power-optimized applications.[9]

Mn is even more readily available than Ni,[27] and lithium manganese oxide suitable as an insertion material crystallizes in the spinel structure. Also in the spinels, oxygen form a cubic close packed structure, but with a different arrangement of the cations as compared to the layered oxides previously described. The cations fill half of the octahedral and one eight of the tetrahedral cavities, and the cations in octahedral sites are sometimes indicated with brackets in the $A[B]_2O_4$ notation. $Li[Mn]_2O_4$,[37] or "LMO", is a commercialized cathode material for Li-ion batteries. The spinel structure provides channels for Li-ion transport in all three crystallographic directions, and its practical capacity is around 110 mAh/g at an average potential of 4 V. However, it experiences capacity fading during cycling, especially at elevated temperatures due to Mn^{2+} dissolution, formed through disproportionation of Mn^{3+}.[9]

The only commercially available iron-based cathode material for Li-ion batteries is $LiFePO_4$, commonly abbreviated "LFP". It is an electronically insulating material with a very low electrical conductivity of 10^{-9} S/cm at room temperature,[38] and the first report of the material demonstrated unimpressive performance.[39] The electrochemical performance of $LiFePO_4$ was substantially improved by coating the material with a conductive carbon layer,[40,41] leading to its commercialization in the early 2000's. However, the Li-ion conductivity is reported to be even lower than the electronic conductivity, and some researchers claim that small particle size is more important than a conductive carbon coating for $LiFePO_4$.[42,43] The carbon source would then mainly prevent particle growth during the synthesis of $LiFePO_4$. The Li-ion conductivity is reported to lie in the range 10^{-10} to 10^{-11} S/cm at room temperature,[44,45] although there are some discrepancies in the literature. The values reported are largely dependent on the synthesis conditions, and a few percent occupancy of Fe^{2+} in the Li^+ sites create vacancies or Li-Fe anti-site defects in the structure.[46] That could possibly explain why some researchers report Li-ion transport in one crystallographic dimension,[47] just as theoretical work predicts,[48–50] whereas other report two-dimensional Li-ion transport.[44] In any case, nanosizing and carbon coating of the $LiFePO_4$ grains substantially improved its electrochemical performance,[40,41,51,52] and today $LiFePO_4$ is even used in high-power applications.[33]

LFP is taking an increasingly large market share of the commercial cathode materials, but the technology is still dominated by Co and Ni based layered oxides such as LCO, NCA, and NMC. The market shares of commercial cathode materials are summarized in *Figure 3*.[53]

A comparison of the state-of-the art layered oxide (NMC) with the LFP cycled against a lithium anode is shown in *Figure 4*. Neither of these electrodes were optimized, but show characteristic performance of NMC and

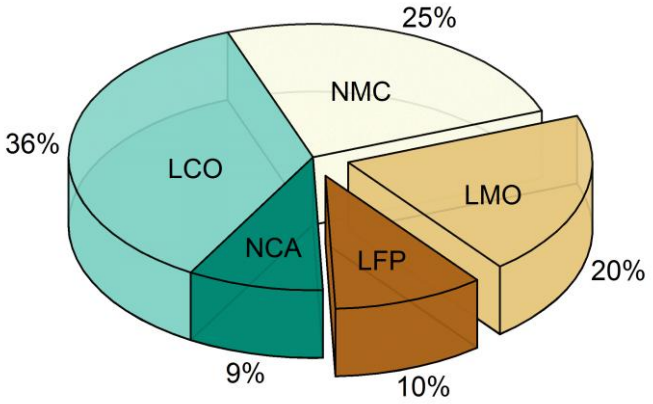

Figure 3. The market share of different commercial cathode materials in Li-ion batteries by weight.[53] The graph includes $LiFePO_4$ (LFP), $LiCoO_2$ (LCO), $LiNiO_2$ doped with Co and Al (NCA) or Mn and Co (NMC), and $LiMn_2O_4$ (LMO).

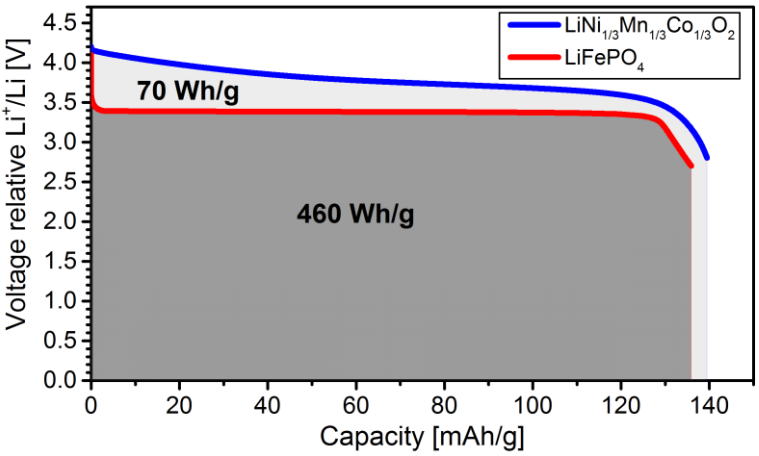

Figure 4. A comparison between laboratory scale batteries with commercial LFP and NMC as cathode material. The batteries were cycled at the rate of C/10 (the NMC data was provided by E. Björklund).

LFP, respectively. The energy storage capacity is about 15% larger by weight for NMC compared to LFP. It remains a task for battery researchers to improve materials based on abundant elements in order to realize cost-effective batteries for electric vehicles and grid applications.

2.2 Future iron based Li-insertion cathodes

As can be anticipated from the description of the commercialized Li-ion batteries in the previous section, Li-ion insertion cathode materials are built up by combination of small insertion metal-ions from the s-block, redox active metal-ions from the d-block, and a simple or polyatomic anion from the p-block in the periodic table. The insertion metal ion (*e.g.* Li^{+}) balances the negative charge from the anions (*e.g.* O^{2-}) in the compound when the transition metal ion is being reduced during discharge (*e.g.* Co^{4+} to Co^{3+}). The transition metals used in layered and spinel oxides are normally Co, Ni, or Mn. Fe and V are the most common transition metals for insertion materials with polyatomic anions, *e.g.* SO_4^{2-}, PO_4^{3-}, or SiO_4^{4-}.[33] As remarked at the end of Section 2.1, commercial Li-ion batteries are still largely based on cobalt containing layered oxides, and it is desirable to replace the Co-ion with the more abundant and less toxic Fe-ion. The following section discusses the possible combinations of the elements in the periodic table to form new compounds suitable for Li-ion battery cathodes. The materials listed in Table 1 will be used as examples when discussing ways to increase the energy density of iron based Li-ion insertion materials.

2.2.1 Lithium iron oxides and the unstable Fe(IV) state

Lithium iron oxide, α-$LiFeO_2$, shows limited capacity and poor cycling performance due to its disordered structure and the instability of the Fe(IV) state.[67,68] Thus, replacing $LiCoO_2$ with an iron based material is not straightforward. Since the sizes of the Li^{+} and Fe^{3+} ions are similar, there is a mixed occupancy of metal ions in the octahedral sites of the cubic closed packed oxygen structure. Thus, the Li-ions are trapped in a disordered rock-salt structure formed for $LiFeO_2$, in contrast to the layered structure of $LiCoO_2$.[69]

Several other types of lithium iron oxides have been reported, but none show attractive electrochemical performance. In addition to the difficulties associated with extracting Li-ions from a disordered rock-salt structure, the rather exotic Fe(IV) oxidation state would have to be form during the delithiation process. Fe^{4+} has been reported in some perovskite materials which contain large divalent cations (Ca^{2+}, Sr^{2+} and Ba^{2+}), *e.g.* in $CaFeO_3$.[75] In those structures the oxide ligands are partly oxidized (sometimes referred to as ligand hole formation), which stabilizes Fe^{4+} in those perovskites.[76,77] This way, the Jahn-Teller distortion otherwise

Table 1. *Theoretical performance of some iron based Li-ion insertion materials.*

Compound	Capacity [mAh/g]	Voltage [V]	Energy density [mWh/g]	Note	Ref.
$LiFeO_2$*	(283)	(3.6)	1019	Limited Li-ion transport. Instability of Fe^{4+}.	[54]
$LiFeF_3$	224	3.2	717	Difficult to synthesize in the lithiated state.	[55,56]
LiFeOF	274	2.8	767	Meta-stable compound.	[57]
$LiFePO_4$	170	3.45	587	Current state-of-the-art Fe based cathode material.	[39,41]
$LiFeBO_3$	220	2.8	616	Air sensitive, slow Li-ion transport.	[58,59]
Tavorite $LiFeSO_4F$	151	3.6	544	Fast Li-ion transport, but low energy density and difficult synthesis.	[60]
Triplite $LiFeSO_4F$	151	3.9	589	High energy density but unfavorable Li-ion transport.	[61,62]
$Li_2FeP_2O_7$*	110 (220)	3.5 (5.0)	385 (935)	Low capacity if only the $Fe^{3+/2+}$ redox couple is utilized.	[63]
$Li_2Fe_2Si_2O_7$	182	3.0?	546?	Unknown. Probably requires exotic synthesis methods.	[64,65]
Li_2FeSiO_4*	166 (331)	2.8 (4.5)	465 (1208)	Based on abundant materials, but low energy density and slow Li-ion transport.	[66]

*Numbers in parenthesis rely on the use of the unstable Fe(IV) state

expected for the $t_{2g}^3e_g^1$ electron configuration for d-block metal ions is avoided.

Interestingly, recent computational studies suggested that *ca.* 10% excess of Li^+ in disordered rock-salt structures, such as α-$LiFeO_2$, leads to a fully percolating network for Li-ion extraction and insertion.[69,78] The prediction recently gained experimental support through studies into the redox activity reported for solid solutions of α-$LiFeO_2$ and Li_2TiO_3, in which replacement of Fe^{3+} with Ti^{4+} creates metal site vacanices.[79] For $x > 0.13$ in $Li_{1+x}Ti_{2x}Fe_{1-3x}O_2$, a simultaneous oxidation of Fe^{3+} to Fe^{4+} and oxidation of oxide ligands was suggested based on X-ray absorption spectroscopy measurements.[79] The suggested electrochemical mechanism is rather exotic, but it has been recently suggested for several Li-ion and Na-ion insertion materials such as $LiMnPO_4$,[80] $Li_2Ru_{1-y}Sn_yO_3$,[81] $Li_{3.5}FeSbO_6$,[82] and α-$NaFeO_2$.[68] The electrochemical cycling of these ternary oxides is more or less stable, but all show some capacity fading when used in batteries. Thus, it is worth noting that the traditional view on redox processes in insertion materials described

on page 7 is a simplification. The compound as a whole, not just the transition metal ion, must be considered in the redox process upon lithium insertion and extraction. Hybridization of metal and ligand orbitals must be considered, and it is the energy difference between the lithiated and delithiated state that determines the thermodynamic voltage of a material. Oxide ligand contributions to redox processes in Li-ion batteries were recently summarized.[83]

It can be concluded that iron oxides show little promise for being used as cathodes in Li-ion batteries. The structural instability and amorphization, together with the instability of the Fe^{4+} ion make the utilization of the $Fe^{4+/3+}$ redox couple challenging. The low voltage of the $Fe^{3+/2+}$ redox couple and the fact that the iron oxides are commonly synthesized in the delithiated discharge state make them unpractical as cathode materials in Li-ion batteries based on the rocking-chair concept.

2.2.2 Lithium iron sulfides, nitrides, and fluorides

Since iron oxides are not alternatives for Li-ion battery cathodes, simple compounds with other electronegative elements could be considered as replacements for oxides. Aiming for high capacity, the weight penalty of the anions should be minimized. A total negative charge of at least minus three is required to balance the positive charge of the Fe^{2+} and Li^{+} cations, and the lightest possible anions are or S^{2-}, N^{3-}, and F^{-}.

Iron sulfides, FeS and FeS_2, have a voltage of *ca*. 2 V relative to Li^{+}/Li, similar to the iron oxides. They do not follow a Li-ion insertion mechanism in contrast to the previously discussed TiS_2, but undergo a conversion reaction upon reduction. Fe and Li_2S are formed upon lithiation, possibly with amorphous Li_2FeS_2 as an intermediate product, and FeS and S_8 are formed upon delithiation.[84,85] The system suffers from the poor electrochemical cyclability often observed for conversion reactions, and parasitic reactions due to the soluble lithium polysulfides well known in Li-S battery research.[86] Starting in the 1970's, batteries with iron sulfide positive electrodes operating at high temperatures were investigated.[87] The final configuration had a LiAl anode and molten LiCl-LiBr-KBr eutectic mixtures as the electrolyte and operated at 400-450°C.[88] The high operating temperature and corrosion problems for the system made it unfavorable as compared to, *e.g.*, room temperature Li-ion batteries and the research interest declined in the 1990's.[12]

There are some reports of iron nitrides for Li-ion battery applications, *e.g.* layered $Li_2(Li_{0.7}Fe_{0.3})N$[89], cubic $Cr_{1-x}Fe_xN$,[90] and hexagonal Fe_3N.[91] However, these nitrides have a voltage of only about 1-2 V relative to Li^{+}/Li, and are not interesting as a cathode materials.[89]

Iron fluorides, FeF_2 and FeF_3, are currently being investigated as cathode materials in Li-ion batteries.[92] In FeF_3, one Li-ion per formula unit is insert-

ed reversibly around 3.3 V relative to Li^+/Li, followed by a conversion reaction to LiF and Fe upon further lithiation at lower potentials.[55] Mixed iron oxide fluorides are also reported in the literature,[57] *i.e.* FeO_xF_{2-x} with $0 < x < 1$. Their electrochemical mechanism is similar to that for FeF_3, but at a voltage around 2.8 V relative to Li^+/Li for the insertion reaction.[57,93] However, neither $LiFeF_3$ nor LiFeOF have been synthesized directly in the lithiated state, which is a requirement for using the materials in a full cell with *e.g.* a graphite anode. It is likely that novel synthesis methods are required to form the lithiated fluorides, such as the recently reported *operando* synthesis of $LiFeF_3$ from nanometer sized LiF and FeF_2.[56] According to Table 1, lithium iron fluorides and oxyfluorides offer the greatest increase in energy density for batteries based on the $Fe^{3+/2+}$ redox couple. The increase corresponds to *ca.* 30% by weight compared to $LiFePO_4$ if new synthesis routes are found.

2.2.3 The inductive effect for polyanionic insertion cathodes

As described in section 2.1, $LiFePO_4$ is the only commercially available iron based cathode for Li-ion batteries. Almost 95% of the 170 mAh/g theoretical capacity can be utilized in a battery, and it operates at a voltage of 3.45 V relative to Li^+/Li. Compared to the iron oxides described in Section 2.2.3, the potential of the $Fe^{3+/2+}$ redox couple is about 1 V higher in $LiFePO_4$. Understanding the increased voltage requires complex thermodynamic consideration, and experimental chemists often use simplified rules-of-thumb in the search for new insertion materials.[94] One such tool is the *inductive effect*. Some other simplified rules for estimating the voltage of $M^{3+/2+}$ redox couples were recently summarized.[94]

The inductive effect is used to describe the distribution of electrons within σ-bonds in a molecule, and is well-known in organic chemistry. The cation *X* in a polyatomic anion XO_4^{n-}, *e.g.* P^{5+} in PO_4^{3-}, pulls electrons from the Fe-O bond *via* the Fe-O-*X* linkage. Since the electron configuration of high-spin Fe^{2+} is $t_{2g}^4e_g^2$, oxidation of Fe^{2+} to Fe^{3+} results from a removal of an electron from the anti-bonding HOMO e_g orbitals. The more covalent the Fe-O bond is, the larger the splitting between the bonding t_{2g} and anti-bonding e_g orbitals becomes, leading to an increased energy of the e_g orbitals and lower redox potential of $Fe^{3+/2+}$. Thus, by increasing the electronegativity of *X*, the Fe-O bond can be tuned to be more ionic, resulting in an increased $Fe^{3+/2+}$ redox potential.

The inductive effect was described by Goodenough and co-workers in the late 1980's.[95] It is supported by experimental data from the NASICON type compounds $Fe_2(XO_4)_3$ with *X*=W, Mo or S,[95,96] $Li_3Fe_2(XO_4)_3$ with *X*=P,[97] and $LiFe_2(SO_4)_2(PO_4)$.[98] Within the same structure type, the potential of the $Fe^{3+/2+}$ redox couple scales fairly linearly with the electronegativity of the

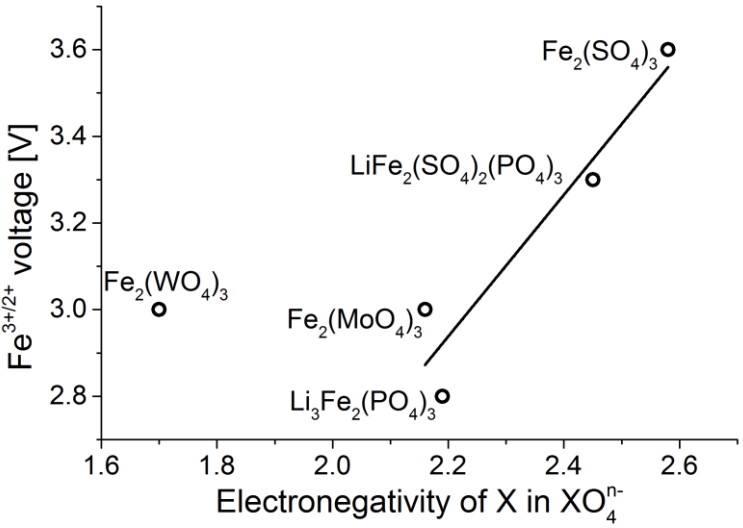

Figure 5. The voltage of the $Fe^{3+/2+}$ redox couple increases with the electronegativity of the cation *X* in polyanionic compounds through the inductive effect.

cation, as shown in *Figure 5*. Other transition metals than Fe also showed similar behaviors.[33] The inductive effect alone is of course a simplified description for the potentials of the $Fe^{3+/2+}$ redox couple, but it still provides useful guidance in predicting the potentials of polyanionic compounds. It does not, however, explain why *tavorite* and the *triplite* polymorph of $LiFeSO_4F$ are oxidized around 3.6 V and 3.9 V, respectively, upon delithiation.[60–62] Neither does it explain why $LiFeP_2O_7$ has a potential of 2.9 V upon lithium insertion,[99] whereas lithium extraction from $Li_2FeP_2O_7$ with a different crystal structure occurs at 3.5 V relative to Li^+/Li.[63]

2.2.4 Alternatives to $LiFePO_4$ based on the $Fe^{3+/2+}$ redox couple

Following the success of $LiFePO_4$, several other polyanionic iron based cathode materials have been discovered, and the subject was recently reviewed.[33] The only known iron based polyanionic compounds that can be synthesized in the lithiated state and which theoretically could outperform $LiFePO_4$[39] in terms of energy density are $LiFeBO_3$[58] and *triplite* $LiFeSO_4F$,[61,62] as summarized in Table 1. In terms of practical energy density, these compounds still have some associated challenges. The borate must not be exposed to air in order to function well in a battery, since air exposure results in material degradation, detrimental for its electrochemical performance.[59] The *triplite* $LiFeSO_4F$ has a disordered structure with no straight channels for Li-ion transport,[100] and utilization of the entire theoretical capacity could not be achieved even *via* chemical oxidation.[100] Still, an ad-

vantage is that it can be synthesized simply through ball-milling with an optional heat treatment at 300°C,[101] possibly reducing its production cost.

Another way to improved cathodes based on polyanionic insertion materials is to aim for materials with fast Li-ion transport, where nanosizing should be less important.[43] Larger particles can be packed more densely, which is beneficial for the volumetric energy density.[10,102] That could provide an opportunity for the *tavorite* polymorph of $LiFeSO_4F$,[60] which has an open crystal framework and fast Li-ion transport according to computational studies.[103] Indeed, it delivers a high practical capacity with low polarization even for micrometer sized particles when coated with an electronically conductive layer.[104]

The condensed lithium iron phosphate, $Li_2FeP_2O_7$, could also be interesting, as it has an open crystal structure with predicted low barrier for Li-ion transport in $Li_2FeP_2O_7$.[105,106] It shows relatively good electrochemical performance even with micron sized particles,[106] and no substantial improvement upon nanosizing,[107] although it suffers from a low gravimetric energy density because of the heavier $P_2O_7^{4-}$ anion.

A condensed silicate, with the $Si_2O_7^{6-}$ would be ideal for balancing two Li^+ and two Fe^{2+} ions while reducing the weight penalty of the polyanion. Additionally, condensed polyanions might reduce the covalency of the Fe-O bond further,[94] increasing the redox potential. $Na_2Mn_2Si_2O_7$ is known and has an open structure,[108] but is formed at high temperatures and pressures. Condensed di-orthosilicates appear to be difficult to synthesize in general. Lithium di-silicate $Li_6Si_2O_7$, which resembles the mineral Åkermanite ($Ca_2MgSi_2O_7$), is a metastable phase formed by rapid cooling.[65] Although Åkermanite is a naturally occurring mineral, it is unlikely that a stable structure is formed with the small Li-ion;[64] its structure is stabilized by larger cations such as Ca^{2+}.

2.2.5 The $Fe^{4+/3+}$ redox couple in polyanionic cathodes

The only way to significantly increase the energy density of polyanionic Li-ion battery cathode materials appears to be to involve more than one oxidation step per transition metal ion.[102] Possible candidates could then be Li_2FeSiO_4[66] and $Li_2FeP_2O_7$.[63] Extracting Li-ions and two electrons from Li_2FeSiO_4 would result in capacity of 331 mAh/g at an average potential around 3.8 V, with the average potential of 2.8 V for the first and 4.5 V for the second oxidation step.[66,109] Thus, the gravimetric energy density would be roughly twice as large as for $LiFePO_4$.

As described in Section2.2.1, only limited redox activity at a potential around 4 V relative to Li^+/Li is reported based on the $Fe^{4+/3+}$ redox couple in iron oxides. Energy storage based on the $Fe^{4+/3+}$ redox couple appears to be at least equally difficult to achieve in polyanionic compounds. Considering that the voltage of the $Fe^{3+/2+}$ redox couple is *ca.* 1 V higher in polyanionic

compounds compared to oxides, and further oxidation occurs around 4 V relative to Li^+/Li for the oxides, the potential of the $Fe^{4+/3+}$ redox couple is likely around 5 V in polyanionic compounds. Indeed, computational studies predict that the second oxidation step would occur around 4.8 V for Li_2FeSiO_4,[110] and around 5 V for $Li_2FeP_2O_7$.[111] Currently, no electrolytes have such a high anodic stability for long term cycling in a battery.[112,113] Additionally, as previously described, the cycling stability for $Fe^{4+/3+}$ involves anionic contributions to the redox activity, which are interesting but presently not stable enough.

For $Li_2FeP_2O_7$, some initial electrochemical results imply a second oxidation step and extraction of the second Li-ion,[111] whereas other studies report no redox activity below 5 V after the complete oxidation of the Fe-ion to Fe^{3+}.[114] Further experimental studies are needed to clarify this matter. On the other hand, a two-step oxidation of Li_2FeSiO_4 has been the subject of a scientific debate recently. Lv *et al*. carried out *in-situ* X-ray absorption (XAS) experiments and observed a shift in the Fe K-edge which could be attributed to the Fe^{4+} ion.[109] Brownrigg *et al*. observed no Fe^{4+} in their XAS data from cells that had been allowed to relax prior to measurements, and they attributed all charge capacity above 4.2 V to electrolyte degradation.[115] Masese *et al*. reported anion oxidation during the second oxidation step for Li_2FeSiO_4, but no Fe^{4+} formation.[116] Still, another *in-operando* XAS study indicated the presence of Fe^{4+} above 4.4 V relative to Li^+/Li.[117] Yang *et al*. reported somewhat reversible Li-ion insertion and extraction corresponding to *ca*. 320 mAh/g but observed no Fe^{4+} based on a combination of *ex-situ* ^{57}Fe Mössbauer spectroscopy and electron spin resonance.[118] They also speculated that oxidation of the oxide ligands was the active redox process for the second oxidation step. Taking all these studies into account, a two-step oxidation process with extraction of two Li-ions per formula unit does not seem impossible for Li_2FeSiO_4. It might be that both Fe^{4+} and ligand holes are formed simultaneously, but that Fe^{4+} is converted to Fe^{3+} in a self-discharge process during relaxation. Such mechanisms have been reported for α-$NaFeO_2$ in Na-ion batteries,[68] and seems to be much faster for Li_2FeSiO_4. In any case, new electrolytes need to be developed for stable battery performance above 4.5 V relative to Li^+/Li.

3 Scope of the thesis

In the work presented here, focus lies on improving and understanding the function of iron based insertion materials for the positive electrode in a Li-ion battery. Three different polyanionic iron based Li-ion insertion materials were investigated in three different papers.

Paper I aims at gaining deeper understanding of structural and electronic properties of $Li_2FeP_2O_7$ upon Li-ion insertion and extraction. A preferential oxidation of iron sites depending on the coordination number was identified. Furthermore, the degree of intermixing between Li- and Fe-ions within the crystal structure was studied. It was found that a metastable state with increased Li-Fe intermixing was formed upon electrochemical cycling.

In *Paper II*, the *tavorite* polymorph of $LiFeSO_4F$ was investigated. Previous work showed that the use of a conductive polymer coating substantially improved the electrochemical function of the material.[104] In Paper II, the effect of the amount of conductive polymer was investigated, and a suitable range of the polymer to $LiFeSO_4F$ weight ratio was identified. Reducing the porosity improved the electronic contact for cast electrodes of polymer coated $LiFeSO_4F$, and it was concluded that sufficient electron transport to the active material grains was essential for the function of the material.

Paper III focuses on the *triplite* polymorph of $LiFeSO_4F$, one of few iron based Li-ion insertion materials that in theory could outperform the commercially available $LiFePO_4$. It was found that the conductive polymer coating improved the electrochemical performance, just as it did for the *tavorite* polymorph in Paper II. Paper III also addresses the effect of temperature on the electrochemical performance of *triplite* $LiFeSO_4F$.

Through the papers, this thesis addresses fundamental aspects of the active material, together with electrode engineering. Such insights are of interest in the design of optimized positive electrodes for Li-ion batteries.

4 Experimental methods

In the following section, the synthesis of iron based Li-ion insertion materials is described, together with a description of the materials characterization techniques used and the electrochemical evaluation.

4.1 Materials synthesis

4.1.1 $Li_2FeP_2O_7$ from solid state synthesis

$Li_2FeP_2O_7$ was synthesized *via* a conventional solid state synthesis route,[63] starting from Li_2CO_3, $(NH_4)_2HPO_4$, and $FeC_2O_4 \cdot 2H_2O$ in the molar ratio 1/2/1. By mixing and heating the reactants, gaseous carbon oxides, water, and ammonia were driven off and crystalline $Li_2FeP_2O_7$ was formed. The reaction must be carried out under an inert atmosphere; impurity phases containing ferric iron were formed if oxygen was present. Sufficient mixing was also essential to prevent the formation of $Li_4P_2O_7$ and $Fe_2P_2O_7$ impurities.

4.1.2 *Tavorite* $LiFeSO_4F$ by solvothermal synthesis

Tavorite $LiFeSO_4F$ was obtained by replacing the water in $FeSO_4 \cdot H_2O$ with LiF in a topotactic reaction.[119,120] The reaction was carried out in tetraethylene glycol (TEG) inside a Teflon lined steel autoclave. Important synthesis parameters include the temperature[121] and the water content in the reaction vessel. If the amount of water increased, the reaction yield was lower.

4.1.3 *Triplite* $LiFeSO_4F$ *via* high-energy ball milling

Triplite $LiFeSO_4F$ was synthesized through high-energy ball milling of anhydrous $FeSO_4$ and LiF under inert atmosphere.[101] A mild heat treatment (270 °C for 7 h) under vacuum increased the crystallinity of the product. As with the other compounds containing ferrous iron, the presence of oxygen leads to formation of impurities. The high local impact during high-energy ball milling in a shaker type equipment was crucial in forming the product.

When the reactants were grinded in a planetary ball mill, no reaction occurred.

4.1.4 Poly(3,4-ethylenedioxythiophene) coatings

A conductive poly(3,4-ethylenedioxythiophene)-bis(trifluoromethane)-sulfonimide coating (PEDOT-TFSI), was synthesized using partly delithiated $LiFeSO_4F$ as the oxidizing agent in the polymerization of EDOT monomers. In the first step, chemical delithiation was carried out under inert atmosphere using nitronium tetrafluoroborate (NO_2BF_4) as the oxidizing agent. The ratio $LiFeSO_4F$:NO_2BF_4 determined the degree of delithiation *x*. In a second step, the polymerization was carried out by evaporating a methanol solution containing EDOT monomers and excess of LiTFSI salt under inert atmosphere. The reaction is simplified below. A p-doping level of +1/3 per repeating unit was assumed.[122,123]

$$Li_{1-x}FeSO_4F + \text{EDOT} + xLi^+ \rightarrow LiFeSO_4F\text{-PEDOT}^{0.33+} \quad [1]$$

4.2 Materials characterization

The sample purity and the structure of crystalline Li-ion insertion materials were determined with powder X-ray diffraction (XRD). PEDOT coatings were qualitatively identified with IR- and Raman spectroscopy, and quantitatively by thermogravimetric analysis (TGA). Mössbauer spectroscopy was used to quantify the amount of ferrous and ferric ions in different crystallographic sites in the samples. Additionally, scanning electron microscopy (SEM) was used to investigate the morphology of the active materials and the electrodes, and X-ray photoelectron spectroscopy was used to investigate changes in the PEDOT coatings upon electrochemical cycling.

The materials characterization techniques used in this thesis are briefly described below, with focus on powder XRD and Mössbauer spectroscopy. More detailed information is available in the specialized literature.[124–129]

4.2.1 Powder XRD

When a wave passes through a grating it is dispersed, and these waves interact through interference. The phenomenon can be observed when the grating distance is of similar magnitude to the wavelength of the incoming wave. In a crystalline solid, the crystallographic planes are separated by distances in the order of 10^{-10} m (1 Å). Electromagnetic radiation with similar wavelengths falls in the X-ray region, so an interference pattern is created when a crystalline solid is irradiated with X-ray radiation. From such interference patterns the crystal structure, *i.e.* the crystal lattice and the atomic positions,

can be obtained. The crystal structure is described by the unit cell, the smallest repeating unit of a periodic crystal containing all symmetry elements.

The basis vectors **a**, **b**, and **c** describe the crystal lattice. The crystallographic planes are then described by their Miller indices *h*, *k*, and *l*, indicating how many equal parts the basis vectors **a**, **b**, and **c** are divided into. The interplanar spacing *d* between the crystallographic planes is determined by Braggs' law (Eq. 2), which is the criterion for constructive interference at a given wavelength λ and at certain diffraction angles θ between the incident X-ray radiation and the crystallographic planes.

$$2d \sin\theta = n\lambda \quad [2]$$

Only the first order interference (n = 1) is considered, as higher order reflections can be described with multiples *n* of the Miller indices. The intensity *I* of the diffracted beam from a Bragg reflection (*hkl)* is determined by the structure factor $|F|^2$ (Eq. 3).

$$I \propto |F|^2(hkl) \quad [3]$$

Thus, the structure amplitude *F* for a given crystallographic plane can be calculated from the diffracted intensity, if geometrical effects are accounted for and the diffracted intensity is normalized to a constant scale factor. *F* is a complex function of the atomic scattering length, population, and the atomic displacement factors of all the atoms in the unit cell. Symmetry elements in the crystal induce systematic extinctions, *i.e.* the structure amplitude is zero for certain crystallographic planes, and the crystal structure can thereby be determined from a diffraction experiment. However, the phase angle between its real and complex part cannot be obtained, since *F* is the square root of the intensity. This complication is referred to as the *phase problem* in crystallography.

For powder XRD, where an almost infinite number of crystallites with random orientation are measured, the diffracted waves fall on the surfaces of diffraction cones. Therefore, powder XRD histograms are normally presented with the intensity as a function of the diffraction angle θ. The unit cell parameters can then be assigned from the position of the Bragg peaks (Eq. 2), and the atomic positions can be determined by evaluating the structure amplitude from the measured intensities. However, solving an unknown crystal structure from powder data is complicated. In addition to the always present phase problem, more than one Bragg peak can have the same angle θ in a powder XRD histogram. Compared to a single crystal measurement, some information is lost when measuring on numerous crystallites simultaneously.

4.2.2 Mössbauer spectroscopy

The Mössbauer effect is the recoilless emission of γ-radiation from a radioactive source and absorption by a sample of interest. Suitable isotopes for Mössbauer spectroscopy exist for many elements but only ^{57}Fe Mössbauer spectroscopy is discussed in this thesis. The following description is largely based on local course material.[130]

The γ-radiation source in ^{57}Fe Mössbauer spectroscopy is typically a radioactive ^{57}Co source inside a metal matrix, *e.g.* ^{57}CoRh. Since the ^{57}Co atoms are locked in the rigid solid source, recoilless emission of radiation with energy suitable for excitation of ^{57}Fe is produced. If the ^{57}Fe nuclei in the absorber also are locked in a solid matrix, recoilless absorption can occur. The electronic and chemical environment around the ^{57}Fe nuclei slightly changes their nucleus energy levels, and the energy from the source is fine-tuned with the Doppler Effect by moving it back and forth with a few mm/s. Thus, information regarding oxidation state, chemical environment, and magnetic properties can be obtained from a Mössbauer spectrum. Absorbance is normally given as a function of energy in mm/s, taking α-Fe as reference.

The nuclear energy levels in the Fe core is affected by several phenomena. Firstly, it is affected by electrostatic interactions with the surrounding electrons. For example, the s-electrons have a rather high probability to penetrate the core, resulting in a slightly different size of the nucleus. This gives rise to the *isomer shift* in Mössbauer spectroscopy, where an increased density of electrons within the Fe core shifts the absorption to lower energies. The absorption energy is also shifted due to atomic vibrations in the source and the sample. The effect is referred to as the *second order Doppler Effect*, which is temperature dependent. The shift in absorption energy for ^{57}Fe at room temperature is a couple of tenths of mm/s. Thus, the shift in γ- absorption is given as the *center shift*, being the sum of the isomer shift and the second order Doppler Effect.

Secondly, since the Fe nucleus is ellipsoidal in the spin quantum state $I = 3/2$, the γ-absorption splits into two energy levels if the electric field at the nucleus is asymmetrical. A doublet is then observed in the Mössbauer spectrum. The asymmetry can be originated from *e.g.* a paramagnetic electronic configuration, and asymmetric configuration of the surrounding ligands. The hyperfine difference between the two absorption energies is referred to as the *quadrupole splitting*.

Finally, the nucleus has a magnetic moment and the energy levels are split into two levels for the ground state (m = +1/2 and -1/2) and four in the excited state (m = +3/2, +1/2, -1/2 and -3/2). Transitions with a change in the magnetic quantum number of ≤ 1 are allowed, giving rise to a Mössbauer sextet for magnetic samples.

4.2.3 Additional characterization techniques

Vibrational spectroscopy

When a sample is irradiated with electromagnetic radiation in the infrared (IR) or visible region, it can be excited to a higher vibrational energy state. If there is a change in the dipole moment during the transition, IR radiation can be absorbed. That process is detected in IR spectroscopy, and the higher the change in the dipole moment is, the stronger the absorption.

In Raman spectroscopy, the sample is irradiated with visible light. The light is then scattered by the sample, either elastically (Rayleigh scattering) or inelastically (Raman scattering). Raman scattering contains the most chemical information of the sample, since the photon energy is changed by the interaction with the sample. In the Stokes band the photon energy is decreased, and in the *anti*-Stokes band the photon energy is increased. Raman scattering occurs when there is a change in polarizability in the electron cloud of the sample

IR and Raman spectroscopy are to great extent complimentary techniques. If there is a center of symmetry in a molecule, the asymmetric vibrational excitations will induce a change in the dipole moment and the compounds are IR active. The transitions to symmetric vibrational modes will change the polarizability of the molecule, and compounds with such vibrational modes are Raman active.

Thermogravimetric analysis (TGA)

In TGA, the weight of a sample is monitored at a controlled temperature, normally during heating. The heating takes place in a furnace under a controlled atmosphere, *e.g.* under nitrogen or oxygen flow. Typically, the weight of the sample is recorded as a function of temperature during a ramp, or as a function of time at a constant temperature. In that way, information regarding material stability and degradation involving changes in mass is obtained.

X-ray photoelectron spectroscopy (XPS)

Core electrons can be emitted from a sample when it is irradiated with X-ray radiation. In XPS, the number of *photoelectrons* is measured as a function of their kinetic energy. The technique is very surface sensitive; the probing depth is typically 10-30 Å depending on the energy of the incoming X-rays. Measurements are normally carried out under ultra-high vacuum to avoid any interactions between emitted photoelectrons and gas molecules. From the kinetic energy, the binding energy of a surface species can be calculated (Eq. 4).

$$h\nu = E_K + E_B + \phi \qquad [4]$$

In [3], $h\nu$ is the energy of the incoming X-ray radiation, E_K is the kinetic energy of the emitted photoelectron, E_B is the binding energy for the electron, and ϕ is a correction term taking into account both instrumental contri-

butions (*e.g.* change in photoelectron energy upon interaction with the detector) and sample contributions (*e.g.* charging of an insulating sample). Thus, the binding energy can be obtained if the sample is irradiated with monochromatic light, after correcting for ϕ with an internal standard.

Scanning electron microscopy (SEM)

By using a focused high energy electron beam instead of visible light, the physical limit of a microscope can significantly enhanced. In SEM, the electron beam is continuously scanned over the sample under vacuum, while detecting backscattered electrons or secondary electrons emitted from the sample. In this work, SEM was used to observe the morphology of Li-ion insertion materials and electrodes. The samples were coated with a thin Cr-layer to prevent charging of the samples.

4.3 Electrochemical evaluation

4.3.1 Battery cell assembly

Batteries were assembled with the material of interest as the working electrode and Li-metal in large excess as a combined counter and reference electrode. If not otherwise stated, the electrolyte was 1 M $LiPF_6$ dissolved in ethylene carbonate (EC) and diethyl carbonate (DEC) in a volume ratio of 1:1. The electrolyte was soaked into a porous membrane, made of either polyethylene or glassfiber, used to prevent short circuiting of the cells.

Both pouch cells and Swagelok cells were assembled. In both cases, the active material was mixed with carbon black to improve their electric contact. The powders were loaded directly into Swagelok cells, or mixed with poly(vinylidene fluoride-co-hexafluoropropylene) (PVdF-HFP) dissolved in n-methyl-2-pyrrolidone, and cast onto an aluminum foil when used in pouch cells. The electrodes were dried at 120 °C for 12 h, and the battery assembly was carried out under an Ar atmosphere in a glovebox.

4.3.2 Electrochemical characterization

The battery function was mainly studied by chronopotentiometry with potential cut-off limits, commonly referred to as galvanostatic cycling in the battery literature. By applying a constant current, the voltage profile of the battery is obtained as a function of the charge stored. The charge stored or delivered is obtained by multiplying the current with the time during charge and discharge, respectively. The ratio of charge stored and delivered gives the Coulombic efficiency. Integration of the voltage with respect to the charge gives the energy stored or delivered by the battery, and their ratio is

the energy efficiency for the battery at a given current. The power delivered can be obtained by multiplying the average voltage during discharge with the applied current. Herein, different currents were used to investigate different galvanostatic cycling conditions. The current applied is reported in C-rate, *i.e.* the reciprocal of the time in hours required to charge or discharge the full theoretical capacity at a given current.

In Paper III, the cell resistance was measured with Electrochemical Impedance Spectroscopy (EIS). A small alternating voltage perturbation of 10 mV was applied to the cell and the alternating current response was recorded. The small voltage perturbation gives a linear current response, so that the cell's impedance can be determined. By scanning over different frequencies, different electrochemical time domains were investigated and ohmic, faradaic, and non-faradaic processes were separated out. Because of the complicated nature of a Li-ion battery electrode, with many different interphases giving rise to capacitive responses, and Li-ion transport in both the solid and liquid state, no equivalent circuits were fitted to the data. The data was instead interpreted qualitatively.

5 Results and discussion

The three iron based cathode materials studied in this thesis, $Li_2FeP_2O_7$ and the *tavorite* and *triplite* polymorphs of $LiFeSO_4F$, each have their own advantageous, challenges, and scientific questions. As discussed in Chapter 2.2, $Li_2FeP_2O_7$ and *tavorite* $LiFeSO_4F$ are more suitable for high-power applications, whereas *triplite* $LiFeSO_4F$ is more interesting for energy optimized applications. Thus, the Results and Discussion section is divided into two parts, discussing materials for power-optimized and energy-optimized batteries separately. Although the research is motivated by its applications, the main focus is still on the fundamental understanding of these systems.

5.1 Materials for high-power applications

With their open crystal frameworks, $Li_2FeP_2O_7$ and *tavorite* $LiFeSO_4F$ have been suggested for power optimized Li-ion batteries.[60,63,131,132] Additionally, fast Li-ion transport should, in theory, make nanosizing less important.[133] Larger particles can be packed more densely which is beneficial for the volumetric energy density.[10,102]

For $Li_2FeP_2O_7$, the electrochemical mechanism upon extraction and insertion of lithium is under debate.[114,134] The changes in crystal structure after one electrochemical cycle, together with preferential oxidation of iron sites with different coordination numbers, were investigated in Paper I. Such information is important in explaining the Li-ion transport in the material, and the cell voltage of the battery.

For electrodes based on *tavorite* $LiFeSO_4F$, it was found essential to provide sufficient electronic conductivity throughout the electrode. The importance of electron transport to the grains was investigated in two ways in Paper II. Firstly, different amount of the electronically conducting polymer PEDOT was coated onto the $LiFeSO_4F$ particles and the materials were evaluated as powders in Swagelok cells. Secondly, cast composite electrodes compressed to different porosities were evaluated in pouch cells.

5.1.1 Changes in $Li_2FeP_2O_7$ upon electrochemical cycling

The lithium ions in $Li_2FeP_2O_7$ are located in wavy, two-dimensional layers in the *bc*-plane, when describing $Li_2FeP_2O_7$ using the space group $P2_1/c$ in

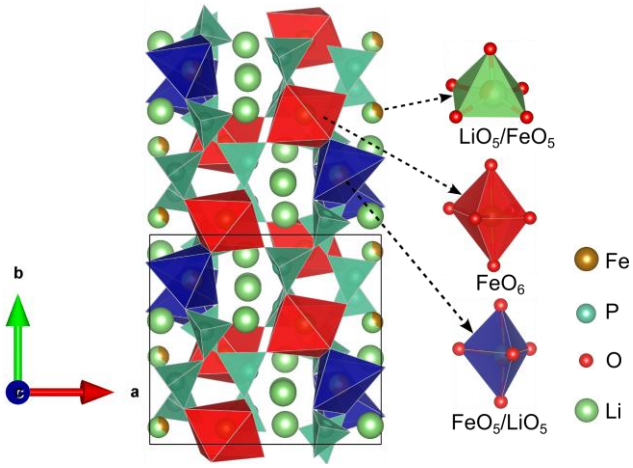

Figure 6. The crystal structure of $Li_2FeP_2O_7$ viewed along the c-axis. Two unit cells are shown.

the monoclinic crystal system. There is also a significant quantity of iron in these lithium layers. One of the five coordinated iron sites is intermixed with a five coordinated lithium site to about 1/3. The crystal structure and Li-Fe intermixing are illustrated in *Figure 6*.

In Paper I it was shown that the amount of Li-Fe intermixing (often entitled "Li-Fe anti-site defects" in the literature) was dramatically increased during electrochemical cycling. The level of intermixing, determined from Rietveld refinement of the XRD patterns in *Figure 7*, increased from about 1/3 to *ca.* 1/2 during the first cycle. Thereafter, the degree of Li-Fe intermixing remained fairly constant upon further cycling, but could be reversed to around 1/3 through annealing the sample at 600 °C post cycling. Such information should be important to describe the Li-ion transport in the material. Computational studies of $Li_2FeP_2O_7$ suggested that the Li-Fe intermixing can provide a path for Li-ion transport between the two-dimensional layers in the structure, making Li-ion transportation in the material three-dimensional.[105] Furthermore, the fact that the initial degree of intermixing, 1/3, could be restored through annealing implies that a metastable state is formed during battery operation. Such a metastable state, with higher free energy than the initial lithiated state before cycling, could be a reason for the lowered electrochemical potential after the first charge.[135] A higher free energy of the lithiated state would make the change in free energy less negative during discharge, resulting in a lower redox potential. It should be recognized, however, that the structure of the delithiated form $LiFeP_2O_7$ is still not known, and changes in that phase upon cycling will of course also affect the cell voltage.

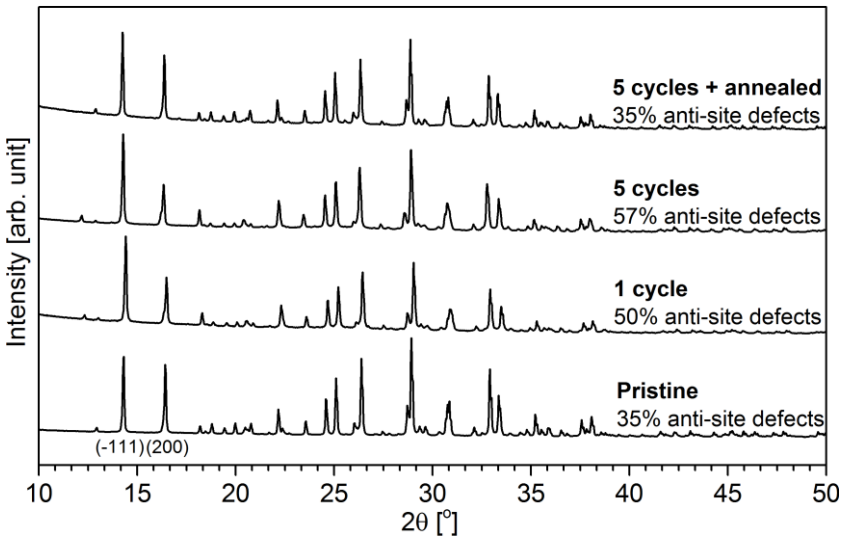

Figure 7. The low-angle part of the diffractograms of $Li_2FeP_2O_7$ at cycled to different extents. The relative intensities of the (-111) and (200) reflections are influenced by electrochemical cycling and annealing *post*-cycling.

Paper I also contains a Mössbauer study, investigating whether the five- or six-coordinated iron sites in the structure are oxidized preferentially at different degrees of delithiation. As shown in *Figure 6*, there are both five and six coordinated iron sites in the structure. It is rare to find such a case for Li-insertion materials, making $Li_2FeP_2O_7$ a suitable model compound for that kind of investigation. It was possible to assign the doublets in the Mössbauer spectra by recognizing that their populations were in the ratio 1:2:3, in agreement with the Li-Fe intermixing determined by powder XRD. A preference for oxidation of the six-coordinated iron site was found at the beginning of charge, followed by the five-coordinated sites at later stages. The finding should be of importance when relating crystal structure to electrochemical potential for insertion materials. For example, since the Fe-O bond is longer (*i.e.* more ionic) at higher coordination numbers, a discussion based on the inductive effect would predict that a five-coordinated site would be oxidized prior to a six-coordinated site. The findings in Paper I show that such reasoning is too simplified.

The findings of the XRD and Mössbauer spectroscopy studies in Paper I are summarized in *Figure 8*. The preferential oxidation of six-coordinated iron at low voltages is shown in red, and five-coordinated iron at higher voltages is shown in blue. Also the increased Li-Fe mixing upon cycling is indicated.

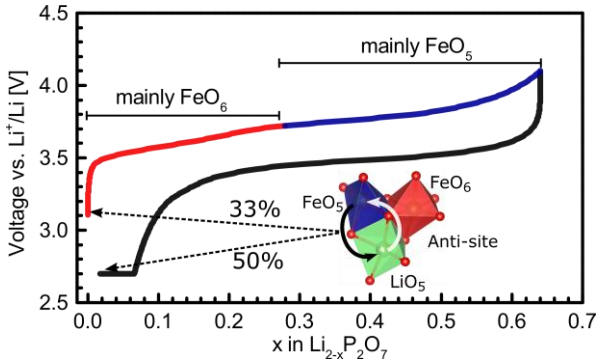

Figure 8. Summary of the findings in Paper I. The degree of Li-Fe intermixing is increased by electrochemical cycling, and the six-coordinated iron is mainly oxidized prior to the five coordinated iron sites.

5.1.2 *Tavorite* $LiFeSO_4F$ electrodes

The *tavorite* $LiFeSO_4F$ has been shown to function well when coated with a conductive polymer, such as p-doped poly(3,4-dioxythiophene)-bis(trifluoromethane)sulfonimide; PEDOT-TFSI.[104] SEM micrographs for *tavorite* $LiFeSO_4F$, pristine and PEDOT-coated, are shown in *Figure 9***.** It was suggested that the electronic conduction pathways to the particles, *via* the conductive PEDOT coating, is important for the function of the material in a Li-ion battery. On the other hand, adding mass in addition to the active material applies a weight penalty on the composite material. Even though PEDOT itself is electrochemically active in the voltage window used for cycling $LiFeSO_4F$, PEDOT has a much lower theoretical capacity. When $TFSI^-$ is used as the counter ion for p-doped PEDOT, the theoretical capacity is only 38 mAh/g. $LiFeSO_4F$, on the other hand, could theoretically deliver 151 mAh/g. Thus, there is a trade-off between favorable electronic conduction and the weight penalty for the heavy polymer.

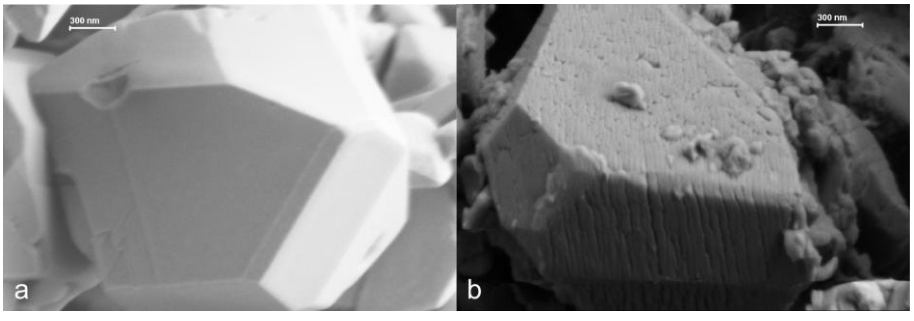

Figure 9. SEM micrographs of pristine (a) and PEDOT-coated (b) *tavorite* *$LiFeSO_4F$* .

In Paper II, micrometer sized *tavorite* $LiFeSO_4F$ particles were coated with 6, 12, and 24% PEDOT. It was found that 12% PEDOT gave the highest practical energy density at low cycling rates, when normalizing against the weight of *both* $LiFeSO_4F$ and PEDOT-TFSI. At higher cycling rates, *i.e.* higher than 1C, the highest level of PEDOT-TFSI gave the best performance. In addition to the improved electric contact with higher PEDOT content, the dilution of $LiFeSO_4F$ results in a lower theoretical capacity of the $LiFeSO_4F$-PEDOT composite, as discussed in Paper II. Thus, with a higher PEDOT-content the applied current at a given C-rate will be lower than for $LiFeSO_4F$ coated with smaller amounts of PEDOT. That could be the explanation for the better performance at higher rates with larger amounts of PEDOT. The findings are summarized in the Ragone plot in *Figure 10*. These investigations were carried out on $LiFeSO_4F$-PEDOT powders mixed with a large amount of carbon black, 15% by weight, and loaded into Swagelok cells with no binder added.

Considering a real battery application, cast composite electrodes are more relevant. However, it has proven difficult to prepare well-performing cast electrodes of *tavorite* $LiFeSO_4F$, both based on previous experience at Uppsala University and in the literature.[136] It was speculated that when the $LiFeSO_4F$ is exposed to moist air during the casting process, it degrades to $FeSO_4 \cdot H_2O$ and LiF which would limit the electrochemical performance.[136] However, the investigations of PEDOT coatings on $LiFeSO_4F$ in Paper II and previous work[104] indicated that electronic conduction is a key factor for

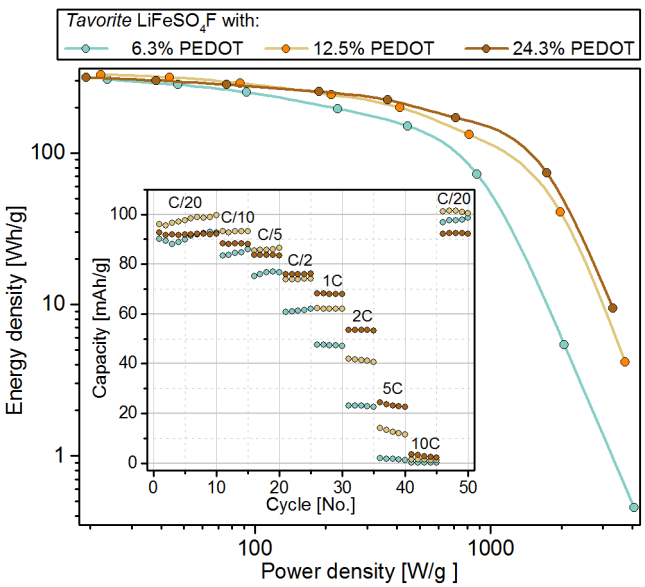

Figure 10. Ragone plot for $LiFeSO_4F$ coated with different amounts of PEDOT-TFSI.

the material. For cast electrodes, electronic conduction can be improved by calendering and densifying the electrodes, which was also investigated in Paper II.

Aiming for high theoretical energy density, cast electrodes comprised of 80% *tavorite* $LiFeSO_4F$ by weight were prepared. The electrode formulation by weight was set to $LiFeSO_4F$/PEDOT/carbon black/binder as 80/7/5/8. The casting process resulted in thin, *ca.* 30 µm thick, electrodes with porosities around 55%. The cycling curves for the first cycle of these electrodes are shown in *Figure 11*, together with post cycling SEM images of the electrodes. The highly porous electrodes showed large polarization**,** and unimpressive capacity retention. However, the electrochemical performance was significantly enhanced by densifying the electrodes. The densest electrodes showed similar cycling as for material loaded as a powder in a Swagelok cells. The dense electrodes did not provide exceptional rate-performance, as Li-ion transport in the electrolyte was likely the limitation for such compact electrodes.[137] Thus, another trade-off, between electronic and ionic conduction is apparent in this case.

The result presented in Paper II point out the crucial role of electronic transport to the *tavorite* $LiFeSO_4F$ grains. The function of the material is improved by both increasing the amount of PEDOT, and by making very dense electrodes.

5.2 Materials for improved energy density

5.2.1 $Li_{2-2y}Fe_{1+y}P_2O_7$

In an attempt to increase the capacity of $Li_2FeP_2O_7$, a test series with partial substitution of Li^+ with Fe^{2+} was carried out. Since the $Fe^{4+/3+}$ redox couple has proved difficult to utilize in polyanionic compounds, as described in the Sections 2.2.1 and 2.2.5, the idea was to increase the amount of Fe^{2+} at

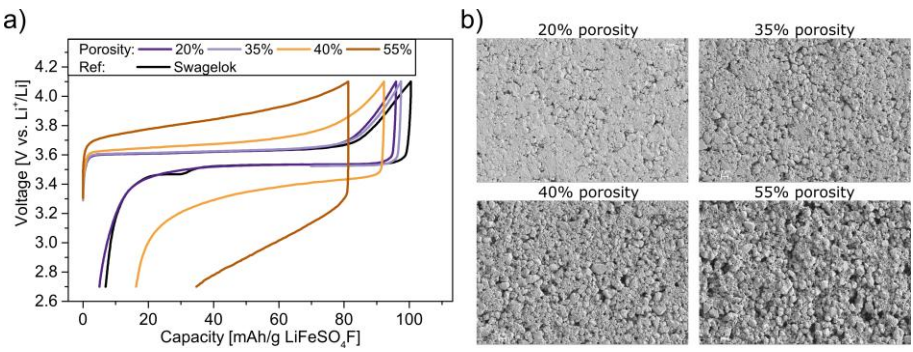

Figure 11. Electrochemical cycling performance at C/20 (a), and the corresponding SEM micrographs (b).

the expense of Li^+ in $Li_2FeP_2O_7$. Since Fe^{2+} and Li^+ are to a large extent intermixed in the five coordinated metal sites in the crystal structure, [63] and since the intermixing increased during lithium extraction and insertion as shown in Paper I, the intended substitution was to replace two Li-ions with one ferrous ion and a vacancy to form $Li_{2-2y}Fe_{1+y}P_2O_7$. Ideally, such a substitution would increase the theoretical capacity to139 mAh/g for $Li_{4/3}Fe_{4/3}P_2O_7$ as compared to 110 mAh/g for $Li_2FeP_2O_7$ when operating based on the $Fe^{3+/2+}$ redox couple.

After the attempted synthesis, powder XRD showed that a mixture of $Li_2FeP_2O_7$ and $Fe_2P_2O_7$ had formed instead of the targeted $Li_{2-2y}Fe_{1+y}P_2O_7$. The amount of $Fe_2P_2O_7$ increased with the attempted degree of substitution y, as indicated by the increased intensity of the strongest reflection of the impurity phase, marked with stars in *Figure 12*. It was concluded that $Li_{2-2y}Fe_{1+y}P_2O_7$ is not the thermodynamically most stable species, possibly due to large electrostatic repulsion between the divalent ions in situated too close proximity to each other, as can be anticipated from the structure model in *Figure 6*.

5.2.2 *Triplite* $LiFeSO_4F$

In Paper III, the effect of coating the *triplite* $LiFeSO_4F$ with electronically conducting PEDOT was investigated, together with the effect of temperature on the electrochemical cycling. The PEDOT coating had a beneficial effect on the electrochemical performance of *triplite* $LiFeSO_4F$ polymorph in a similar way as it had for the *tavorite* polymorph in Paper II and in the literature[104]. The practical capacities increased and polarization decreased. However, the improvement was not as significant as for the *tavorite* polymorph.

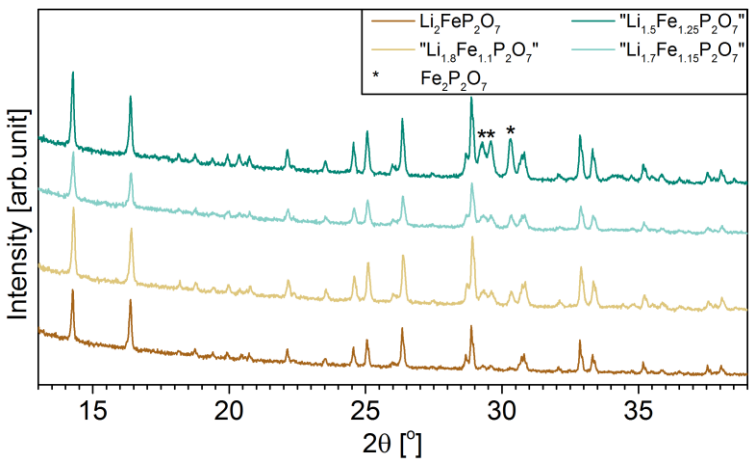

Figure 12. Powder XRD results for attempts to synthesize $Li_{2-2y}Fe_{1+y}P_2O_7$. The strongest reflections of the impurity phase $Fe_2P_2O_7$ are indicated by stars.

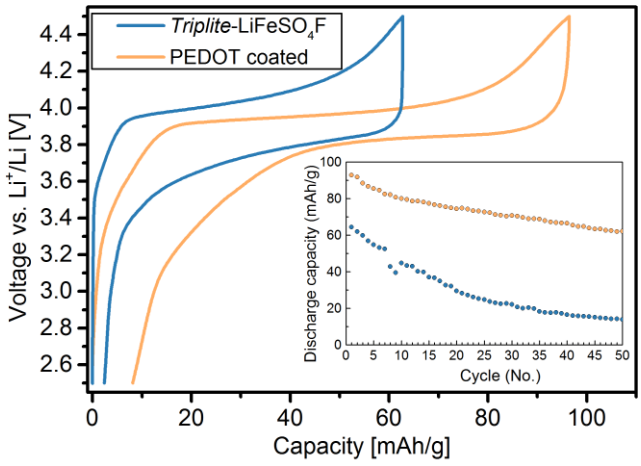

Figure 13. Electrochemical cycling at C/20 for *triplite* $LiFeSO_4F$ with and without PEDOT coating.

The electrochemical cycling of pristine and PEDOT coated *triplite* $LiFeSO_4F$ is presented in *Figure 13*, and can be compared with the cycling curves in Paper II.

In an attempt to improve the electrochemical performance of PEDOT coated *triplite* $LiFeSO_4F$, cycling at elevated temperatures was carried out. Li-ion conductivity generally increases exponentially with temperature, following an Arrhenius behavior. With an activation energy of 0.5 eV, typical for Li-ion insertion materials such as $LiFePO_4$,[44,47] an increase in temperature from room temperature to 60 °C increases the Li-ion conductivity by approximately one order of magnitude. It should be mentioned that electronic conductivity of insulators and semiconductors also follow an Arrhenius behavior,[138] and also increase exponentially with increasing temperature.

When cycling the material at 60 °C, the polarization was further reduced and the capacity increased, as shown in *Figure 14*. Whether the improved cycling at elevated temperature is due to improved ionic or electronic transport is difficult to evaluate. Not much is reported in the literature regarding transport properties in *triplite* $LiFeSO_4F$. The only report is a computational study comparing the *tavorite* and *triplite* polymorphs of $LiFeSO_4F$[139]. The activation barrier for Li-ion conductivity was not predicted to be much lower for the *triplite* polymorph as compared with the *tavorite* polymorph. However, the authors predicted that the Li-ion conductivity could be lower in *triplite* $LiFeSO_4F$, as it appeared to occur in one or two crystallographic directions in contrast to the three dimensional Li-ion transport in *tavorite* $LiFeSO_4F$.

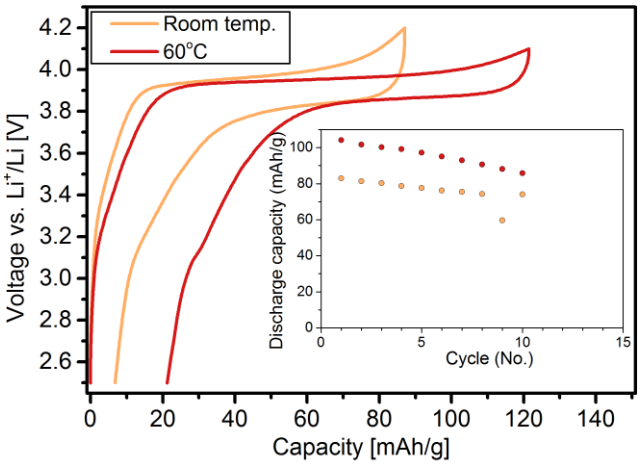

Figure 14. PEDOT coated *Triplite* $LiFeSO_4F$ cycled at C/20 at 60°C and room temperature.

The cycling stability at 60 °C was poor, and after ten to fifteen cycles at C/20 the upper cut-off voltage was never reached during the lithiation, indicating corrosion of the aluminum current collector. Aluminum corrosion was also supported by the severe damage of the current collector observed when disassembling the cells. Electrolytes based on LiBOB salt was used in this study, since they have been shown stable up to 80 °C for electrochemical cycling of $LiFePO_4$.[140] However, the 0.5 V increase in operating potential of *triplite* $LiFeSO_4F$ compared to $LiFePO_4$ seems to induce stability issues. An extended study of suitable electrolytes for electrochemical cycling *triplite* at elevated temperatures is needed.

Finding an electrolyte stable at both high temperatures and high voltages is a challenge.[112,113,141] Standard electrolytes with $LiPF_6$ salt are not stable at 60°C, so electrolytes with LiTFSI salt are often used at 60°C. However, they corrode the aluminum current collector at higher voltages. The $LiBF_4$ salt might improve the passivation of the aluminum current collector.[140] Alternatively, if the solvent is the problem, sulfone based solvents such as tetramethylenesulfone (TMS) have been suggested in the literature.[142] Polymer electrolytes and room temperature ionic liquids are also under development and might be interesting for high temperature cycling.[113,141]

6 Conclusion and outlook

The work presented here addresses both fundamental properties of iron based Li-ion insertion materials, and electrode formulation and engineering. In Paper I, iron atoms with higher coordination number were found to oxidize at later stages of charge of $Li_2FeP_2O_7$. Additionally, an increased intermixing of Li and Fe upon electrochemical cycling was observed. Such findings are important for the understanding of the materials function in a Li-ion battery.

In Paper II and III it was found that a conductive PEDOT coating improved the electrochemical performance of both *tavorite* and *triplite* $LiFeSO_4F$. For micrometer sized particles, *ca.* 10% (w/w) PEDOT was required for a sufficient coating. For cast electrodes with *tavorite* $LiFeSO_4F$ the electrical conduction was also improved by densifying the porous electrode. For *triplite* $LiFeSO_4F$ reducing the particle size and finding an electrolyte that functions well at 3.9 V or higher during long-term cycling at 60° should be investigated in order to improve the electrochemical performance of the material.

From the literature study in Chapter 2, it can be argued that it is not realistic to increase the energy density of iron based Li-ion insertion materials by more than 5-10% based on the $Fe^{3+/2+}$ redox couple. Reports on anionic contribution to charge storage in insertion materials are interesting and should be investigated further. However, future improvements are likely to come from electrode, cell, and battery pack engineering. One way would be to reduce the amount of inactive material in the battery cell by controlling the porosity of cast electrodes and making the cast thicker. Such studies were partly carried out for *tavorite* $LiFeSO_4F$ in Paper II and should be continued. Increasing the temperature window for Li-ion batteries could be another way to improve the battery system for electric vehicles. Reducing the need of cooling the batteries would reduce the weight of the battery system on a vehicle level.

Apart from these practical issues concerning improved Li-ion batteries, there are still many unanswered fundamental questions regarding both $Li_2FeP_2O_7$ and $LiFeSO_4F$. Crystallographically, their structures are not fully investigated during Li-ion extraction and insertion. Electrochemical studies of *e.g.* rate limiting steps of the compounds and battery cells are necessary to improve Li-ion batteries for high-power applications further.

7 Acknowledgements

First and foremost I would like to acknowledge my supervisor, Fredrik, for giving me advice and guidance as well as a large scientific freedom. I would also like to thank my co-supervisors Torbjörn and Carl for a great support and many fruitful discussions.

Thank you to everyone in the SSF project *From Road to Load*, the project funding this work. I am grateful to Kristina for welcoming me at the ÅABC.

Thank you Adam for a good collaboration and many interesting discussions about the nature of iron based cathodes. Thank you Tore and Lennart for your enthusiasm and help with Mössbauer spectroscopy. It is fun working with you. Mario, you always help out no matter what! And I am thankful to Mohammed for introducing me to the world of inorganic synthesis. Thank you Leif for proof reading this thesis and for asking tricky questions that expands my thinking. Thank you Sara, for making me feel welcome in the group and sharing good times both in Uppsala and abroad. I would also like to acknowledge the rest of the COBRA group: Fredde, Wei, and Charlotte. My excellent office mates Tim and Chao deserve special thanks

Thank you Matt for sharing your vast knowledge of both electrochemistry and Finnish Sauna (let's bring it to 100°C!). I am also grateful to Will for giving me insight into understand crystallography and the life down-under, for fun trips, and for proof reading this thesis. I would like to thank the Balcony Boys Stéven, Bertrand, and Mats for many memorable moments. Thank you Solveig for always being helpful and throwing nice dinners and parties. And Julia, Viktor, Fabian, Reza, Jonas and Kasia, and all other nice people in the Friday after work group: you have made my time in Uppsala much more fun. Thank you Gabi and Alina for being the good and reliable people you are and for welcoming me to your wedding. David! It has been nice hanging out with you, both for pleasure and for work. And Linus, Kristina, Martin, Johan C and Johan G, and the rest of the Jobbgympa crew for making the Mondays much more fun. Thank you Habtom for sharing all the small curiosities that we encounter in the lab. And I am grateful to you Anti for helping me think clearly about battery materials and for being an overall nice person. Ronnie, it was nice sharing the Gnarp experience with you! And thank you Henrik, Håkan, and Anders for great support in the lab.

Finally, I would like to thank everyone in the battery group, ND at Structural and Inorganic Chemistry: researchers, technicians, administrative staff, fellow students, and all other good people at Chemistry Ångström

8 References

(1) Clerici, A.; Assayag, M. *World Energy Resouces, 2013 Survey: Summary*; World Energy Council: London, 2013.

(2) Agency, I. E. IEA Sankey Diagram http://www.iea.org/Sankey/index.html#?c=World&s=Balance (accessed Nov 19, 2015).

(3) Dunn, B.; Kamath, H.; Tarascon, J.-M. *Science* **2011**, *334*, 928–935.

(4) Carrasco, J. M.; Franquelo, L. G.; Bialasiewicz, J. T.; Galvan, E.; PortilloGuisado, R. C.; Prats, M. A. M.; Leon, J. I.; Moreno-Alfonso, N. *IEEE Trans. Ind. Electron.* **2006**, *53*, 1002–1016.

(5) Yang, Z.; Zhang, J.; Kintner-Meyer, M. C. W.; Lu, X.; Choi, D.; Lemmon, J. P.; Liu, J. *Chem. Rev.* **2011**, *111*, 3577–3613.

(6) Kempton, W.; Tomić, J. *J. Power Sources* **2005**, *144*, 280–294.

(7) Tarascon, J. M.; Armand, M. *Nature* **2001**, *414*, 359–367.

(8) Reddy, T. *Linden's Handbook of Batteries*; 4th ed.; McGraw-Hill Professional Publishing: New York, NY, USA, 2010.

(9) Croguennec, L.; Palacin, M. R. *J. Am. Chem. Soc.* **2015**, *137*, 3140–3156.

(10) Goodenough, J. B.; Park, K.-S. *J. Am. Chem. Soc.* **2013**, *135*, 1167–1176.

(11) Gamble, F. R.; Osiecki, J. H.; Cais, M.; Pisharody, R.; DiSalvo, F. J.; Geballe, T. H. *Science.* **1971**, *174*, 493–497.

(12) Whittingham, M. S. *Chem. Rev.* **2004**, *104*, 4271–4302.

(13) Yung-Fang Yu Yao; Kummer, J. T. *J. Inorg. Nucl. Chem.* **1967**, *29*, 2453–2475.

(14) Whittingham, M. S.; Huggins, R. A. *J. Chem. Phys.* **1971**, *54*, 414–416.

(15) Whittingham, M. S. *Science.* **1976**, *192*, 1126–1127.

(16) Murphy, D. W.; Trumbore, F. A. *J. Cryst. Growth* **1977**, *39*, 185–199.

(17) Broadhead, J.; Trumbore, F. A.; Basu, S. *J. Electroanal. Chem.* **1981**, *118*, 241–250.

(18) Xu, W.; Wang, J.; Ding, F.; Chen, X.; Nasybulin, E.; Zhang, Y.; Zhang, J.-G. *Energy Environ. Sci.* **2014**, *7*, 513–537.

(19) Rao, B. M. L.; Francis, R. W.; Christopher, H. A. *J. Electrochem. Soc.* **1977**, *124*, 1490.

(20) Obrovac, M. N.; Chevrier, V. L. *Chem. Rev.* **2014**, *114*, 11444–11502.

(21) Mizushima, K.; Jones, P. C.; Wiseman, P. J.; Goodenough, J. B. *Mater. Res. Bull.* **1980**, *15*, 783–789.
(22) Yazami, R.; Touzain, P. *J. Power Sources* **1983**, *9*, 365–371.
(23) Fong, R.; von Sacken, U.; Dahn, J. R. *J. Electrochem. Soc.* **1990**, *137*, 2009.
(24) Peled, E. *J. Electrochem. Soc.* **1979**, *126*, 2047.
(25) Nishi, Y. *J. Power Sources* **2001**, *100*, 101–106.
(26) Yamada, A. *MRS Bull.* **2014**, *39*, 423–428.
(27) British Geological Survey. *Risk List 2012*; 2012.
(28) Delmas, C.; Fouassier, C.; Hagenmuller, P. *Phys. B* **1980**, *99*, 81–85.
(29) Delmas, C.; Peres, J. P.; Rougier, A.; Demourgues, A.; Weill, F.; Chadwick, A. V.; Broussely, M.; Perton, F.; Biensan, P.; Willmann, P. *J. Power Sources* **1997**, *68*, 120–125.
(30) Delmas, C.; Ménétrier, M.; Croguennec, L.; Saadoune, I.; Rougier, A.; Pouillerie, C.; Prado, G.; Grüne, M.; Fournès, L. *Electrochim. Acta* **1999**, *45*, 243–253.
(31) Ohzuku, T.; Yanagawa, T.; Kouguchi, M.; Ueda, A. *J. Power Sources* **1997**, *68*, 131–134.
(32) Madhavi, S.; Subba Rao, G. .; Chowdari, B. V. .; Li, S. F. . *J. Power Sources* **2001**, *93*, 156–162.
(33) Masquelier, C.; Croguennec, L. *Chem. Rev.* **2013**, *113*, 6552–6591.
(34) Lu, Z.; MacNeil, D. D.; Dahn, J. R. *Electrochem. Solid-State Lett.* **2001**, *4*, A191.
(35) Ohzuku, T.; Makimura, Y. *Chem. Lett.* **2001**, 642–643.
(36) Yabuuchi, N.; Ohzuku, T. *J. Power Sources* **2003**, *119-121*, 171–174.
(37) Thackeray, M. M.; David, W. I. F.; Bruce, P. G.; Goodenough, J. B. *Mater. Res. Bull.* **1983**, *18*, 461–472.
(38) Delacourt, C.; Laffont, L.; Bouchet, R.; Wurm, C.; Leriche, J.-B.; Morcrette, M.; Tarascon, J.-M.; Masquelier, C. *J. Electrochem. Soc.* **2005**, *152*, A913–A921.
(39) Padhi, A. K.; Nanjundaswamy, K. S.; Goodenough, J. B. *J. Electrochem. Soc.* **1997**, *144*, 1188–1194.
(40) Ravet, N.; Chouinard, Y.; Magnan, J. F.; Besner, S.; Gauthier, M.; Armand, M. *J. Power Sources* **2001**, *97-98*, 503–507.
(41) Armand, M.; Gauthier, M.; Magnan, J.-F.; Ravet, N. Method for synthesis of carbon-coated redox materials with controlled size. WO0227823 (A1), 2001.
(42) Delacourt, C.; Poizot, P.; Levasseur, S.; Masquelier, C. *Electrochem. Solid-State Lett.* **2006**, *9*, A352.
(43) Gaberscek, M.; Dominko, R.; Jamnik, J. *Electrochem. Commun.* **2007**, *9*, 2778–2783.
(44) Amin, R.; Balaya, P.; Maier, J. *Electrochem. Solid-State Lett.* **2007**, *10*, A13–A16.
(45) Li, J.; Yao, W.; Martin, S.; Vaknin, D. *Solid State Ionics* **2008**, *179*, 2016–2019.

(46) Janssen, Y.; Santhanagopalan, D.; Qian, D.; Chi, M.; Wang, X.; Hoffmann, C.; Meng, Y. S.; Khalifah, P. G. *Chem. Mater.* **2013**, *25*, 4574–4584.
(47) Li, J.; Yao, W.; Martin, S.; Vaknin, D. *Solid State Ionics* **2008**, *179*, 2016–2019.
(48) Morgan, D.; Van der Ven, A.; Ceder, G. *Electrochem. Solid-State Lett.* **2004**, *7*, A30–A32.
(49) Ouyang, C.; Shi, S.; Wang, Z.; Huang, X.; Chen, L. *Phys. Rev. B* **2004**, *69*, 104303.
(50) Islam, M. S.; Driscoll, D. J.; Fisher, C. A. J.; Slater, P. R. *Chem. Mater.* **2005**, *17*, 5085–5092.
(51) Yamada, A.; Chung, S. C.; Hinokuma, K. *J. Electrochem. Soc.* **2001**, *148*, A224.
(52) Huang, H.; Yin, S.-C.; Nazar, L. F. *Electrochem. Solid-State Lett.* **2001**, *4*, A170.
(53) Pillot, C. Battery Market Development for Consumer Electronics, Automotive and Industrial: Materials Requirements and Trends www.avicenne.com (accessed Sep 21, 2015).
(54) Takeda, Y.; Nakahara, K.; Nishijima, M.; Imanishi, N.; Yamamoto, O.; Takano, M.; Kanno, R. *Mater. Res. Bull.* **1994**, *29*, 659–666.
(55) Badway, F.; Cosandey, F.; Pereira, N.; Amatucci, G. G. *J. Electrochem. Soc.*, 2003, *150*, A1318.
(56) Kim, S.-W.; Nam, K.-W.; Seo, D.-H.; Hong, J.; Kim, H.; Gwon, H.; Kang, K. *Nano Today* **2012**, *7*, 168–173.
(57) Pereira, N.; Badway, F.; Wartelsky, M.; Gunn, S.; Amatucci, G. G. *J. Electrochem. Soc.* **2009**, *156* , A407–A416.
(58) Legagneur, V.; An, Y.; Mosbah, A.; Portal, R.; Le Gal La Salle, A.; Verbaere, A.; Guyomard, D.; Piffard, Y. *Solid State Ionics* **2001**, *139*, 37–46.
(59) Yamada, A.; Iwane, N.; Harada, Y.; Nishimura, S.; Koyama, Y.; Tanaka, I. *Adv. Mater.* **2010**, *22*, 3583–3587.
(60) Recham, N.; Chotard, J.-N.; Dupont, L.; Delacourt, C.; Walker, W.; Armand, M.; Tarascon, J.-M. *Nat. Mater.* **2010**, *9*, 68–74.
(61) Liu, L.; Zhang, B.; Huang, X. *Prog. Nat. Sci. Mater. Int.* **2011**, *21*, 211–215.
(62) Barpanda, P.; Ati, M.; Melot, B. C.; Rousse, G.; Chotard, J.-N.; Doublet, M.-L.; Sougrati, M. T.; Corr, S. A.; Jumas, J.-C.; Tarascon, J.-M. *Nat. Mater.* **2011**, *10*, 772–779.
(63) Nishimura, S.; Nakamura, M.; Natsui, R.; Yamada, A. *J. Am. Chem. Soc.* **2010**, *132*, 13596–13597.
(64) Kusaka, K.; Hagiya, K.; Ohmasa, M.; Okano, Y.; Mukai, M.; Iishi, K.; Haga, N. *Phys. Chem. Miner.* **2001**, *28*, 150–166.
(65) Völlenkle, H.; Wittmann, A.; Nowotny, H. *Monatshefte fur Chemie* **1969**, *100*, 295–303.
(66) Nytén, A.; Abouimrane, A.; Armand, M.; Gustafsson, T.; Thomas, J.

O. *Electrochem. Commun.* **2005**, *7*, 156–160.
(67) Kanno, R.; Shirane, T.; Inaba, Y.; Kawamoto, Y. *J. Power Sources* **1997**, *68*, 145–152.
(68) Lee, E.; Brown, D. E.; Alp, E. E.; Ren, Y.; Lu, J.; Woo, J.-J.; Johnson, C. S. *Chem. Mater.* **2015**, *27*, 6755–6764.
(69) Urban, A.; Lee, J.; Ceder, G. *Adv. Energy Mater.* **2014**, *4*, 1400478.
(70) Kanno, R. *J. Electrochem. Soc.* **1996**, *143*, 2435.
(71) Armstrong, A. R.; Tee, D. W.; La Mantia, F.; Novák, P.; Bruce, P. G. *J. Am. Chem. Soc.* **2008**, *130*, 3554–3559.
(72) Chen, C. J.; Greenblatt, M.; Waszczak, J. V. *J. Solid State Chem.* **1986**, *64*, 240–248.
(73) Thackeray, M. M.; David, W. I. F.; Goodenough, J. B. *Mater. Res. Bull.* **1982**, *17*, 785–793.
(74) Amine, K.; Yasuda, H.; Yamachi, M. *J. Power Sources* **1999**, *81-82*, 221–223.
(75) Kanamaru, F.; Miyamoto, H.; Mimura, Y.; Koizumi, M.; Shimada, M.; Kume, S.; Shin, S. *Mater. Res. Bull.* **1970**, *5*, 257–261.
(76) Zaanen, J.; Sawatzky, G. A.; Allen, J. W. *Phys. Rev. Lett.* **1985**, *55*, 418–421.
(77) Bocquet, A. E.; Fujimori, A.; Mizokawa, T.; Saitoh, T.; Namatame, H.; Suga, S.; Kimizuka, N.; Takeda, Y.; Takano, M. *Phys. Rev. B* **1992**, *45*, 1561–1570.
(78) Lee, J.; Urban, A.; Li, X.; Su, D.; Hautier, G.; Ceder, G. *Science.* **2014**, *343*, 519–522.
(79) Glazier, S. L.; Li, J.; Zhou, J.; Bond, T.; Dahn, J. R. *Chem. Mater.* **2015**, *27*, 7751.
(80) Hollmark, H. M.; Gustafsson, T.; Edström, K.; Duda, L.-C. *Phys. Chem. Chem. Phys.* **2011**, *13*, 20215.
(81) Sathiya, M.; Rousse, G.; Ramesha, K.; Laisa, C. P.; Vezin, H.; Sougrati, M. T.; Doublet, M.-L.; Foix, D.; Gonbeau, D.; Walker, W.; Prakash, A. S.; Ben Hassine, M.; Dupont, L.; Tarascon, J.-M. *Nat. Mater.* **2013**, *12*, 827–835.
(82) McCalla, E.; Sougrati, M. T.; Rousse, G.; Berg, E. J.; Abakumov, A.; Recham, N.; Ramesha, K.; Sathiya, M.; Dominko, R.; Van Tendeloo, G.; Novák, P.; Tarascon, J.-M. *J. Am. Chem. Soc.* **2015**, *137*, 4804–4814.
(83) Grimaud, A.; Hong, W. T.; Shao-Horn, Y.; Tarascon, J.-M. *Nat. Mater.* **2016**, *15*, 121–126.
(84) Golodnitsky, D.; Peled, E. *Electrochim. Acta* **1999**, *45*, 335–350.
(85) Zhang, S. S. *J. Mater. Chem. A* **2015**, *3*, 7689–7694.
(86) Yang, Y.; Zheng, G.; Cui, Y. *Chem. Soc. Rev.* **2013**, *42*, 3018.
(87) Vissers, D. R.; Tomczuk, Z.; Steunenberg, R. K. *J. Electrochem. Soc.* **1974**, *121*, 665.
(88) Henriksen, G. L.; Vissers, D. R. *J. Power Sources* **1994**, *51*, 115–128.

(89) Rowsell, J. L. C.; Pralong, V.; Nazar, L. F. *J. Am. Chem. Soc.* **2001**, *123*, 8598–8599.
(90) Sun, Q.; Fu, Z.-W. *Electrochem. Solid-State Lett.* **2008**, *11*, A233.
(91) Fu, Z.-W.; Wang, Y.; Yue, X.-L.; Zhao, S.-L.; Qin, Q.-Z. *J. Phys. Chem. B* **2004**, *108*, 2236–2244.
(92) Conte, D. E.; Pinna, N.; Berlin, H.; Chemie, I. *Mater. Renew. Sustain. Energy* **2014**, *3*, 1–40.
(93) Zhou, Y.-N.; Sina, M.; Pereira, N.; Yu, X.; Amatucci, G. G.; Yang, X.-Q.; Cosandey, F.; Nam, K.-W. *Adv. Funct. Mater.* **2015**, *25*, 696–703.
(94) Gutierrez, A.; Benedek, N. A.; Manthiram, A. *Chem. Mater.* **2013**, *25*, 4010–4016.
(95) Manthiram, A.; Goodenough, J. B. *J. Power Sources* **1989**, *26*, 403–408.
(96) Manthiram, A.; Goodenough, J. B. *J. Solid State Chem.* **1987**, *71*, 349–360.
(97) Masquelier, C.; Padhi, A. K.; Nanjundaswamy, K. S.; Goodenough, J. B. *J. Solid State Chem.* **1998**, *135*, 228–234.
(98) Padhi, A. K. *J. Electrochem. Soc.* **1998**, *145*, 1518.
(99) Padhi, A. K.; Nanjundaswamy, K. S.; Masquelier, C.; Okada, S.; Goodenough, J. B. *J. Electrochem. Soc.* **1997**, *144*, 1609.
(100) Ati, M.; Melot, B. C.; Chotard, J.-N.; Rousse, G.; Reynaud, M.; Tarascon, J.-M. *Electrochem. Commun.* **2011**, *13*, 1280–1283.
(101) Ati, M.; Sathiya, M.; Boulineau, S.; Reynaud, M.; Abakumov, A.; Rousse, G.; Melot, B.; Van Tendeloo, G.; Tarascon, J.-M. *J. Am. Chem. Soc.* **2012**, *134*, 18380–18387.
(102) Berg, E. J.; Villevieille, C.; Streich, D.; Trabesinger, S.; Novák, P. *J. Electrochem. Soc.* **2015**, *162*, A2468–A2475.
(103) Tripathi, R.; Gardiner, G. R.; Islam, M. S.; Nazar, L. F. *Chem. Mater.* **2011**, *23*, 2278–2284.
(104) Sobkowiak, A.; Roberts, M. R.; Younesi, R.; Ericsson, T.; Tai, C.; Andersson, A. M.; Häggström, L.; Tai, C.; Andersson, A. M.; Edström, K.; Gustafsson, T.; Björefors, F. *Chem. Mater.* **2013**, *25*, 3020–3029.
(105) Lee, S.; Park, S. S. *Chem. Mater.* **2012**, *24*, 3550–3557.
(106) Clark, J. M.; Nishimura, S.; Yamada, A.; Islam, M. S. *Angew. Chemie Int. Ed.* **2012**, *51*, 13149–13153.
(107) Barpanda, P.; Ye, T.; Chung, S.-C.; Yamada, Y.; Nishimura, S.; Yamada, A. *J. Mater. Chem.* **2012**, *22*, 13455–13459.
(108) Astakhov, L. P.; Pobedims, E. A.; Simonov, V. I. *Dokl. Akad. Nauk SSSR* **1967**, *173*, 1401–1403.
(109) Lv, D.; Bai, J.; Zhang, P.; Wu, S.; Li, Y.; Wen, W.; Jiang, Z.; Mi, J.; Zhu, Z.; Yang, Y. *Chem. Mater.* **2013**, *25*, 2014–2020.
(110) Seo, D.-H.; Kim, H.; Park, I.; Hong, J.; Kang, K. *Phys. Rev. B* **2011**, *84*, 220106.

(111) Zhou, H.; Upreti, S.; Chernova, N. a.; Hautier, G.; Ceder, G.; Whittingham, M. S. *Chem. Mater.* **2011**, *23*, 293–300.
(112) Xu, K. *Chem. Rev.* **2004**, *104*, 4303–4418.
(113) Xu, K. *Chem. Rev.* **2014**, *114*, 11503–11618.
(114) Shimizu, D.; Nishimura, S.; Barpanda, P.; Yamada, A. *Chem. Mater.* **2012**, *24*, 2598−2603.
(115) Brownrigg, A. W.; Mountjoy, G.; Chadwick, A. V.; Alfredsson, M.; Bras, W.; Billaud, J.; Armstrong, A. R.; Bruce, P. G.; Dominko, R.; Kelder, E. M. *J. Mater. Chem. A* **2015**, *3*, 7314–7322.
(116) Masese, T.; Tassel, C.; Orikasa, Y.; Koyama, Y.; Arai, H.; Hayashi, N.; Kim, J.; Mori, T.; Yamamoto, K.; Kobayashi, Y.; Kageyama, H.; Ogumi, Z.; Uchimoto, Y. *J. Phys. Chem. C* **2015**, *119*, 10206–10211.
(117) Kamon-in, O.; Buakeaw, S.; Klysubun, W.; Limphirat, W.; Srilomsak, S. *Int. J. Electrochem. Sci.* **2014**, *9*, 4257–4267.
(118) Yang, J.; Kang, X.; He, D.; Zheng, A.; Pan, M.; Mu, S. *J. Mater. Chem. A* **2015**, *3*, 16567–16573.
(119) Tripathi, R.; Ramesh, T. N.; Ellis, B. L.; Nazar, L. F. *Angew. Chem. Int. Ed. Engl.* **2010**, *49*, 8738–8742.
(120) Eriksson, R.; Sobkowiak, A.; Ångström, J.; Sahlberg, M.; Gustafsson, T.; Edström, K.; Björefors, F. *J. Power Sources* **2015**, *298*, 363–368.
(121) Sobkowiak, A. $LiFeSO_4F$ as a Cathode Material for Lithium-Ion Batteries: Synthesis, Structure, and Function, Doctorial Thesis, Uppsala University, 2015.
(122) Arbizzani, C.; Mastragostino, M.; Rossi, M. *Electrochem. commun.* **2002**, *4*, 545–549.
(123) Jonas, F.; Heywang, G.; Schmidtberg, W.; Heinze, J.; Dietrich, M. Polythiophenes, process for their preparation and their use. EP0339340 (A2), 1989.
(124) Pecharsky, V. K.; Zavalij, P. Y. *Fundamentals of Powder Diffraction and Structural Characterization of Materials*; 2nd ed.; Springer Science & Business Media, 2008.
(125) Gutlich Philipp, Bill Sckhard, T. A. X. *Mössbauer Spectroscopy and Transition Metal Chemistry, Fundamentals and Applications*; Springer: Heidelberg; Berlin, 2011.
(126) Nakamoto, K. *Infrared and Raman spectra of inorganic and coordination compounds*; 6th ed.; Wiley: Hoboken, N.J, 2009.
(127) Haines, P. J. *Principles of Thermal Analysis and Calorimetry*; Royal Society of Chemistry: Cambridge, 2002.
(128) Hüfner, S. *Photoelectron Spectroscopy*; 3rd revise.; Springer Science & Business Media, 2003.
(129) Egerton, R. F. *Physical principles of electron microscopy: an introduction to TEM, SEM, and AEM*; Springer: New York, NY, 2005.
(130) Ericsson, T. *Mössbauer in Uppsala*; Local Course Material, Uppsala,

2015.
(131) Barpanda, P.; Nishimura, S.; Yamada, A. *Adv. Energy Mater.* **2012**, *2*, 841–859.
(132) Rousse, G.; Tarascon, J. M. *Chem. Mater.* **2014**, *26*, 394–406.
(133) Gaberscek, M.; Dominko, R.; Jamnik, J. *Electrochem. commun.* **2007**, *9*, 2778–2783.
(134) Kim, H.; Lee, S.; Park, Y.-U.; Kim, H.; Kim, J.; Jeon, S.; Kang, K. *Chem. Mater.* **2011**, *23*, 3930–3937.
(135) Aydinol, M. K.; Kohan, A. F.; Ceder, G.; Cho, K.; Joannopoulos, J. *Phys. Rev. B* **1997**, *56*, 1354–1365.
(136) Zhang, L.; Tarascon, J.-M.; Sougrati, M. T.; Rousse, G.; Chen, G. *J. Mater. Chem. A* **2015**, *3*, 16988–16997.
(137) Fongy, C.; Gaillot, A.-C.; Jouanneau, S.; Guyomard, D.; Lestriez, B. *J. Electrochem. Soc.* **2010**, *157*, A885.
(138) Atkins, P. *Shriver & Atkins' Inorganic Chemistry*; 5th ed.; Oxford University Press: Oxford, 2010.
(139) Lee, S.; Park, S. S. *J. Phys. Chem. C* **2014**, *118*, 12642–12648.
(140) Zhang, S. S.; Xu, K.; Jow, T. R. *J. Power Sources* **2006**, *159*, 702–707.
(141) Kalhoff, J.; Eshetu, G. G.; Bresser, D.; Passerini, S. *ChemSusChem* **2015**, *8*, 2154–2175.
(142) Li, S.; Zhao, Y.; Shi, X.; Li, B.; Xu, X.; Zhao, W.; Cui, X. *Electrochim. Acta* **2012**, *65*, 221–227.